Journal of Zhejiang University-SCIENCE A (Applied Physics & Engineering)
ISSN 1673-565X (Print); ISSN 1862-1775 (Online)
www.zju.edu.cn/jzus; www.springerlink.com
E-mail: jzus@zju.edu.cn

Exact free vibration analysis of open circular cylindrical shells by the method of reverberation-ray matrix*

Xiong-liang YAO, Dong TANG†, Fu-zhen PANG†‡, Shuo LI

(*College of Shipbuilding Engineering, Harbin Engineering University, Harbin 150001, China*)

†E-mail: tangdong@hrbeu.edu.cn; pangfuzhen@hrbeu.edu.cn

Received June 27, 2015; Revision accepted Oct. 19, 2015; Crosschecked Mar. 10, 2016

Abstract: This paper is concerned with the free vibration analysis of open circular cylindrical shells with either the two straight edges or the two curved edges simply supported and the remaining two edges supported by arbitrary classical boundary conditions. Based on the Donnell-Mushtari-Vlasov thin shell theory, an analytical solution of the traveling wave form along the simply supported edges and the modal wave form along the remaining two edges is obtained. With such a unidirectional traveling wave form solution, the method of the reverberation-ray matrix is introduced to derive the equation of natural frequencies of the shell with different classical boundary conditions. The exact solutions for natural frequencies of the open circular cylindrical shell are obtained with the employment of a golden section search algorithm. The calculation results are compared with those obtained by the finite element method and the methods in the available literature. The influence of length, thickness, radius, included angle, and the boundary conditions of the open circular cylindrical shell on the natural frequencies is investigated. The exact calculation results can be used as benchmark values for researchers to check their numerical methods and for engineers to design structures with thin shell components.

Key words: Open circular cylindrical shell, Method of reverberation-ray matrix, Free vibration analysis, Donnell-Mushtari-Vlasov thin shell theory, Analytical wave form solution

http://dx.doi.org/10.1631/jzus.A1500191 **CLC number:** O327; TB633; U663.2

1 Introduction

Thin shells are extensively used in naval architecture and ocean engineering, as well as in civil, mechanical, and aeronautical engineering. Open circular cylindrical shells (OCCSs) are often used as structural components of pressure vessels, roof structures, open space buildings, and marine structures. It is of great significance for engineers to be familiar with the vibration behaviors of such shell structures in practical design.

Many pioneering scholars have developed numerous approximate analytical models for thin shells. Most thin shell theories developed before 1973 were formulated by Leissa (1973). In subsequent decades many studies of the vibration of OCCSs have been carried out. Early research mainly used numerical approaches such as the Rayleigh-Ritz method (Sewall, 1967; Leissa and Narita, 1984), the finite element method (FEM) (Cantin and Clough, 1968; Lakis and Selmane, 2000), and the finite strip method (Cheung *et al.*, 1989). Exact solutions for determining the natural frequencies of OCCSs were presented in (Suzuki and Leissa, 1986; Lim and Liew, 1995; Yu *et al.*, 1995; Price *et al.*, 1998; Ye *et al.*, 2014a). A wave propagation approach is introduced by Zhang *et al.* (2001) to carry out frequency analysis of cylindrical panels. Free vibration analyses of stiffened cylindrical shallow shells are

‡ Corresponding author

* Project supported by the National Natural Science Foundation of China (Nos. 51209052, 51279038, and 51479041), the Natural Science Foundation of Heilongjiang Province (No. QC2011C013), and the Opening Funds of State Key Laboratory of Ocean Engineering of Shanghai Jiao Tong University (No. 1307), China

ORCID: Dong TANG, http://orcid.org/0000-0003-4586-5609

presented in (Mecitoglu and Dokmeci, 1992; Nayak and Bandyopadhyay, 2002; Zhang and Xiang, 2006). Vibration behaviors of anisotropic OCCSs are analyzed by Selmane and Lakis (1997a; 1997b) and Toorani and Lakis (2001). Recently, much attention has been paid to vibration analysis of laminated, composite or functionally graded OCCSs (Qatu, 2002; Singh and Shen, 2005; Qatu *et al.*, 2010; Su *et al.*, 2014; Ye *et al.*, 2014b).

As far we are aware, research on the vibration analysis of plate-shell coupled structures is rare, especially any using analytical methods. From the literature, it appears that the accuracy of approximate methods is lower than that of analytical methods. The available analytical methods are sometimes too targeted for shell structures to be consistent with exact solutions of other structural components, such as beams and plates. The method of reverberation-ray matrix (MRRM) is suitable for determining the natural frequencies and steady-state response of multi-span structures and space frame structures with complex geometry. MRRM was first proposed by Howard and Pao (1998) and Pao *et al.* (1999) to analyze wave propagation in planar trusses. Subsequently, Pao and his associates extended the method to study waves propagating in multilayered media (Pao *et al.*, 2000; Su *et al.*, 2002; Guo and Chen, 2008; Tian and Xie, 2009). Much attention was paid to applications of MRRM for dynamic analysis of frames and beams (Tian *et al.*, 2003; Chen *et al.*, 2005; Liu *et al.*, 2006; Yu, 2007a; 2007b; Guo *et al.*, 2008; Jiang *et al.*, 2011; Qiao and Chen, 2011; Miao *et al.*, 2013; Guo and Fang, 2014). MRRM is also employed to analyze unidirectional wave propagation through plates (Li *et al.*, 2005; Liu and Xie, 2005; Liu *et al.*, 2010; 2011a; Zhu *et al.*, 2011; 2012; Li *et al.*, 2012, Yu *et al.*, 2012) and closed shells (Tian and Su, 2000; Liu *et al.*, 2011b; 2013). Recently, MRRM has been directed towards the study of functionally graded or laminated structures (Zhou *et al.*, 2009; Li *et al.*, 2012; Liu *et al.*, 2013; Miao *et al.*, 2013; 2015). It is aimed to obtain a unidirectional traveling wave form solution for OCCSs, which is of good consistency with the solutions for beams and plates presented in (Yu, 2007a; 2007b; Jiang, 2011; Liu *et al.*, 2010; 2011a). Therefore, the formulation presented in this paper should prove to be fundamental for vibration analysis of ring-stiffened OCCSs and plate-shell coupled structures.

This paper extends MRRM to the dynamic analysis of OCCSs. Based on the Donnell-Mushtari-Vlasov (DMV) thin shell theory, the free vibration equation of the OCCS with either two simply supported straight edges or two simply supported curved edges is solved to obtain an analytical solution of the traveling wave form along the simply supported edges and the modal wave form along the remaining two edges. With these solutions expressed in matrix form, the scattering matrix, phase matrix, and permutation matrix as well as the reverberation-ray matrix of the OCCS are derived. Then, the equation of natural frequencies of the OCCS is obtained and subsequently solved by the golden section search algorithm (Press *et al.*, 1992; Vajda, 2007). Finally, the method presented in this paper is validated by comparing the calculation results with those obtained by FEM and the method of Leissa (1973). In addition, the effects of shell length, shell radius, shell thickness, and the included angle as well as the classical boundary conditions such as simply supported edge (SSE), clamped edge (CE), and free edge (FE) for the remaining two edges on the natural frequencies are investigated.

2 Formulation

Consider an isotropic OCCS with length L, included angle θ_0, uniform thickness h, middle surface radius R, Young's modulus E, Poisson's ratio μ, and mass density ρ shown in Fig. 1. The axial, circumferential, and radial displacements of the middle surface of the OCCS with reference to the coordinate system are denoted as $u(x, \theta, t)$, $v(x, \theta, t)$, and $w(x, \theta, t)$, respectively. Either the two straight edges or the two curved edges of the shell are assumed to be simply supported in the following discussion. The problem at hand is to determine the natural frequencies of the OCCS.

To begin with, the expressions of the force and moment resultants in terms of the displacement components and the governing equations based on the DMV thin shell theory are introduced. Subsequently, with the employment of a Fourier transform, an analytical solution of the traveling wave form along the simply supported edges and the modal wave form along the remaining two edges is

obtained in the frequency domain. Then, the solutions of the displacements and the force and moment resultants are expressed in matrix form. Finally, the equation of natural frequencies of the OCCS with various classical boundary conditions is obtained by MRRM and solved by the golden section search algorithm. The above-mentioned formulation is presented in detail as follows.

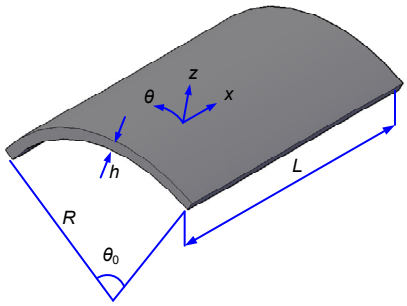

Fig. 1 Geometry and coordinate system for an OCCS

2.1 Force and moment resultants in the shell

The force and moment resultants in an OCCS, shown in Fig. 2, are expressed in terms of the displacements u, v, and w as follows (Leissa, 1973):

$$N_{xx}=C\left(\frac{\partial u}{\partial x}+\frac{\mu}{R}\frac{\partial v}{\partial \theta}+\frac{\mu}{R}w\right), \tag{1}$$

$$N_{\theta\theta}=C\left(\frac{1}{R}\frac{\partial v}{\partial \theta}+\mu\frac{\partial u}{\partial x}+\frac{w}{R}\right), \tag{2}$$

$$N_{x\theta}=N_{\theta x}=C\frac{1-\mu}{2}\left(\frac{1}{R}\frac{\partial u}{\partial \theta}+\frac{\partial v}{\partial x}\right), \tag{3}$$

$$M_{xx}=-D\left(\frac{\partial^2 w}{\partial x^2}+\frac{\mu}{R^2}\frac{\partial^2 w}{\partial \theta^2}\right), \tag{4}$$

$$M_{\theta\theta}=-D\left(\frac{1}{R^2}\frac{\partial^2 w}{\partial \theta^2}+\mu\frac{\partial^2 w}{\partial x^2}\right), \tag{5}$$

$$M_{x\theta}=M_{\theta x}=-D\frac{1-\mu}{R}\frac{\partial^2 w}{\partial x\partial \theta}, \tag{6}$$

$$\begin{aligned}Q_{xz}&=\frac{\partial M_{xx}}{\partial x}+\frac{1}{R}\frac{\partial M_{\theta x}}{\partial \theta}\\&=-D\left(\frac{\partial^3 w}{\partial x^3}+\frac{1}{R^2}\frac{\partial^3 w}{\partial x\partial \theta^2}\right),\end{aligned} \tag{7}$$

$$\begin{aligned}Q_{\theta z}&=\frac{\partial M_{x\theta}}{\partial x}+\frac{1}{R}\frac{\partial M_{\theta\theta}}{\partial \theta}\\&=-D\left(\frac{1}{R^3}\frac{\partial^3 w}{\partial \theta^3}+\frac{1}{R}\frac{\partial^3 w}{\partial x^2\partial \theta}\right),\end{aligned} \tag{8}$$

$$\begin{aligned}F_{x\theta}&=N_{x\theta}+\frac{M_{x\theta}}{R}\\&=\frac{1-\mu}{2}D\left(\frac{12}{h^2}\frac{1}{R}\frac{\partial u}{\partial \theta}+\frac{12}{h^2}\frac{\partial v}{\partial x}-\frac{2}{R^2}\frac{\partial^2 w}{\partial x\partial \theta}\right),\end{aligned} \tag{9}$$

$$F_{\theta x}=N_{\theta x}=C\frac{1-\mu}{2}\left(\frac{1}{R}\frac{\partial u}{\partial \theta}+\frac{\partial v}{\partial x}\right), \tag{10}$$

$$\begin{aligned}V_{xz}&=Q_{xz}+\frac{1}{R}\frac{\partial M_{x\theta}}{\partial \theta}\\&=-D\left(\frac{\partial^3 w}{\partial x^3}+\frac{2-\mu}{R^2}\frac{\partial^3 w}{\partial x\partial \theta^2}\right),\end{aligned} \tag{11}$$

$$\begin{aligned}V_{\theta z}&=Q_{\theta z}+\frac{\partial M_{\theta x}}{\partial x}\\&=-D\left(\frac{1}{R^3}\frac{\partial^3 w}{\partial \theta^3}+\frac{2-\mu}{R}\frac{\partial^3 w}{\partial x^2\partial \theta}\right),\end{aligned} \tag{12}$$

where u, v, and w denote the displacement components in the axial (x), circumferential (θ), and radial (z) directions, respectively. $C=Eh/(1-\mu^2)$ and $D=Eh^3/[12(1-\mu^2)]$ represent the middle surface stiffness and the bending stiffness of the shell. N_{xx} and $N_{\theta\theta}$ denote the in-plane normal forces, $N_{x\theta}$ and $N_{\theta x}$, the in-plane shear forces, M_{xx} and $M_{\theta\theta}$, the bending moments, $M_{x\theta}$ and $M_{\theta x}$, the torsional moments, and Q_{xz} and $Q_{\theta z}$, the out-of-plane shear forces acting on the cross-sections perpendicular to the axial and circumferential directions. $F_{x\theta}$ and $F_{\theta x}$ indicate the in-plane shear force resultants, and V_{xz} and $V_{\theta z}$, the out-of-plane shear force resultants acting on the cross-sections perpendicular to the axial and circumferential directions.

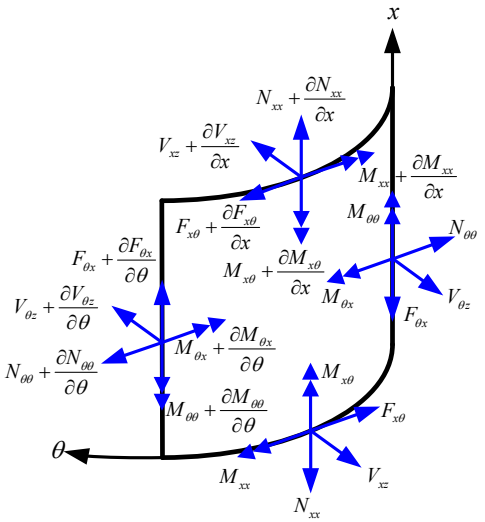

Fig. 2 Force and moment resultants in a shell

2.2 Governing differential equations

The governing differential equations for free vibration of an OCCS based on the DMV thin shell theory can be written as (Leissa, 1973)

$$\frac{\partial^2 u}{\partial x^2}+\frac{1-\mu}{2R^2}\frac{\partial^2 u}{\partial \theta^2}+\frac{1+\mu}{2R}\frac{\partial^2 v}{\partial x\partial \theta}+\frac{\mu}{R}\frac{\partial w}{\partial x}-\frac{(1-\mu^2)\rho}{E}\frac{\partial^2 u}{\partial t^2}=0, \tag{13}$$

$$\frac{1-\mu}{2}\frac{\partial^2 v}{\partial x^2}+\frac{1}{R^2}\frac{\partial^2 v}{\partial \theta^2}+\frac{1+\mu}{2R}\frac{\partial^2 u}{\partial x\partial \theta}+\frac{1}{R^2}\frac{\partial w}{\partial \theta}-\frac{(1-\mu^2)\rho}{E}\frac{\partial^2 v}{\partial t^2}=0, \tag{14}$$

$$R^2\lambda\left(\frac{\partial^4 w}{\partial x^4}+\frac{1}{R^4}\frac{\partial^4 w}{\partial \theta^4}+\frac{2}{R^2}\frac{\partial^4 w}{\partial x^2\partial \theta^2}\right)+\left(\frac{w}{R^2}+\frac{\mu}{R}\frac{\partial u}{\partial x}+\frac{1}{R^2}\frac{\partial v}{\partial \theta}\right)+\frac{(1-\mu^2)\rho}{E}\frac{\partial^2 w}{\partial t^2}=0, \tag{15}$$

where $\lambda=h^2/(12R^2)$ is a dimensionless parameter, which is related to the ratio of shell thickness to radius.

The Fourier transform of an arbitrary physical quantity $X(t)$ is defined by

$$\tilde{X}(\omega)=\int_{-\infty}^{+\infty}X(t)\mathrm{e}^{-\mathrm{i}\omega t}\mathrm{d}t, \tag{16}$$

where ω is the circular frequency, and a tilde over a symbol represents the corresponding quantity expressed in the frequency domain. The inverse Fourier transform is given by

$$X(t)=\frac{1}{2\pi}\int_{-\infty}^{+\infty}\tilde{X}(\omega)\mathrm{e}^{\mathrm{i}\omega t}\mathrm{d}\omega. \tag{17}$$

Taking the Fourier transforms of Eqs. (13)–(15) and eliminating the other two displacement components from the Fourier transforms of Eqs. (13)–(15), three independent equations of motion respectively in terms of $\tilde{u}$, $\tilde{v}$, and $\tilde{w}$ are obtained as follows:

$$\left(L_1L_2L_3L_4+\frac{1}{R^4\lambda}\frac{1-\mu}{1+\mu}L_5L_6\right)\frac{\partial \tilde{u}}{\partial x}=0, \tag{18}$$

$$\left(L_1L_2L_3L_4+\frac{1}{R^4\lambda}\frac{1-\mu}{1+\mu}L_5L_6\right)\frac{\partial \tilde{v}}{R\partial \theta}=0, \tag{19}$$

$$\left(L_1L_2L_3L_4+\frac{1}{R^4\lambda}\frac{1-\mu}{1+\mu}L_5L_6\right)\frac{1}{R}\frac{\partial^2 \tilde{w}}{\partial x\partial \theta}=0, \tag{20}$$

where $\tilde{u}$, $\tilde{v}$, and $\tilde{w}$ denote the axial, circumferential, and radial displacement components expressed in the frequency domain. $\gamma=\{[R^2k_L{}^2-(1-\mu)/(1+\mu)]/(\lambda R^4)\}^{1/4}$ is a parameter of the same dimension with the wave number. L_j (j=1, 2, …, 6) are linear differential operators defined as follows:

$$L_1=\frac{\partial^2}{\partial x^2}+\frac{1}{R^2}\frac{\partial^2}{\partial \theta^2}+\gamma^2, \tag{21}$$

$$L_2=\frac{\partial^2}{\partial x^2}+\frac{1}{R^2}\frac{\partial^2}{\partial \theta^2}-\gamma^2, \tag{22}$$

$$L_3=\frac{\partial^2}{\partial x^2}+\frac{1}{R^2}\frac{\partial^2}{\partial \theta^2}+k_L^2, \tag{23}$$

$$L_4=\frac{\partial^2}{\partial x^2}+\frac{1}{R^2}\frac{\partial^2}{\partial \theta^2}+\frac{2}{1-\mu}k_L^2, \tag{24}$$

$$L_5=\mu\frac{\partial^2}{\partial x^2}-\frac{1}{R^2}\frac{\partial^2}{\partial \theta^2}+\frac{2\mu}{1-\mu}k_L^2, \tag{25}$$

$$L_6=(2+\mu)\frac{\partial^2}{\partial x^2}+\frac{1}{R^2}\frac{\partial^2}{\partial \theta^2}+\frac{2}{1-\mu}k_L^2, \tag{26}$$

where $k_L=\omega[(1-\mu^2)\rho/E]^{1/2}$.

It can be observed from Eqs. (18)–(20) that, the differences among the linear differential operators operating on the axial, circumferential, and radial displacement components lie in the parts outside the braces, which represent zero wave number solutions, or in other words, the rigid-body motions. As normal in free vibration analysis, the zero wave number solutions will be neglected throughout this paper.

2.3 Solutions for OCCS with simply supported curved edges

As the two curved edges of the OCCS are assumed to be simply supported, the boundary conditions at x=0 and x=L are given by (Leissa, 1973)

$$v=0,\ w=0,\ N_{xx}=0,\ M_{xx}=0,\quad x=0,L. \tag{27}$$

According to the boundary conditions defined by Eq. (27), the axial, circumferential, and radial displacements of the OCCS can be written as

$$\tilde{u}(x,\theta)=\sum_{m=1}^{\infty}U(\theta)\cos\left(k_x x\right), \tag{28}$$

$$\tilde{v}(x,\theta)=\sum_{m=1}^{\infty}V(\theta)\sin\left(k_x x\right), \tag{29}$$

$$\tilde{w}(x,\theta)=\sum_{m=1}^{\infty}W(\theta)\sin\left(k_x x\right), \tag{30}$$

where $k_x=m\pi/L$ denotes the wave number in the axial direction, m is the axial mode number, and L represents the length of the OCCS.

Assuming that the axial, circumferential, and radial displacement components can be expressed by exponential functions of the circumferential variable θ, a common circumferential wave number equation for the axial, circumferential, and radial displacements of the OCCS is obtained as

$$\begin{aligned}&\left(k_\theta^2+R^2k_x^2-R^2\gamma^2\right)\left(k_\theta^2+R^2k_x^2+R^2\gamma^2\right)\\&\times\left(k_\theta^2+R^2k_x^2-R^2k_L^2\right)\left(k_\theta^2+R^2k_x^2-\frac{2}{1-\mu}R^2k_L^2\right)\\&-\frac{1}{\lambda}\frac{1-\mu}{1+\mu}\left(k_\theta^2-\mu R^2k_x^2+\frac{2\mu}{1-\mu}R^2k_L^2\right)\\&\times\left[k_\theta^2+(2+\mu)R^2k_x^2-\frac{2}{1-\mu}R^2k_L^2\right]=0.\end{aligned} \tag{31}$$

By solving Eq. (31), eight circumferential wave numbers are obtained:

$$k_\theta=\pm k_{\theta1},\ \pm k_{\theta2},\ \pm k_{\theta3},\ \pm k_{\theta4}. \tag{32}$$

Therefore, the solutions of the equations of motion of the OCCS with two simply supported curved edges are expressed as

$$\tilde{u}(x,\theta)=\sum_{m=1}^{\infty}\sum_{j=1}^{4}\alpha_j\left(a_j\mathrm{e}^{\mathrm{i}k_{\theta j}\theta}+d_j\mathrm{e}^{-\mathrm{i}k_{\theta j}\theta}\right)\cos\left(k_x x\right), \tag{33}$$

$$\tilde{v}(x,\theta)=\sum_{m=1}^{\infty}\sum_{j=1}^{4}\beta_j\left(a_j\mathrm{e}^{\mathrm{i}k_{\theta j}\theta}-d_j\mathrm{e}^{-\mathrm{i}k_{\theta j}\theta}\right)\sin\left(k_x x\right), \tag{34}$$

$$\tilde{w}(x,\theta)=\sum_{m=1}^{\infty}\sum_{j=1}^{4}\left(a_j\mathrm{e}^{\mathrm{i}k_{\theta j}\theta}+d_j\mathrm{e}^{-\mathrm{i}k_{\theta j}\theta}\right)\sin\left(k_x x\right), \tag{35}$$

where a_j and d_j (j=1, 2, 3, 4) are amplitudes of the axial and circumferential waves. α_j and β_j (j=1, 2, 3, 4) are ratios of the amplitudes of the axial and circumferential waves to the amplitude of the radial wave. The expressions of α_j and β_j are defined as follows:

$$\alpha_j=\frac{-Rk_x\left(k_{\theta j}^2-\mu R^2k_x^2+\dfrac{2\mu R^2k_L^2}{1-\mu}\right)}{\left(k_{\theta j}^2+R^2k_x^2-R^2k_L^2\right)\left(k_{\theta j}^2+R^2k_x^2-\dfrac{2R^2k_L^2}{1-\mu}\right)}, \tag{36}$$

$$\beta_j=\frac{\mathrm{i}k_{\theta j}\left(k_{\theta j}^2+(2+\mu)R^2k_x^2-\dfrac{2R^2k_L^2}{1-\mu}\right)}{\left(k_{\theta j}^2+R^2k_x^2-R^2k_L^2\right)\left(k_{\theta j}^2+R^2k_x^2-\dfrac{2R^2k_L^2}{1-\mu}\right)}. \tag{37}$$

The rotation of the normal to the middle surface of the OCCS about the axial direction is defined as

$$\phi_\theta=\frac{v}{R}-\frac{\partial w}{R\partial\theta}. \tag{38}$$

Substituting Eqs. (34) and (35) into the Fourier transform of Eq. (38) yields the frequency domain expression of the rotation as

$$\tilde{\phi}_\theta=\sum_{m=1}^{\infty}\sum_{j=1}^{4}\frac{\beta_j-\mathrm{i}k_{\theta j}}{R}\left(a_j\mathrm{e}^{\mathrm{i}k_{\theta j}\theta}-d_j\mathrm{e}^{-\mathrm{i}k_{\theta j}\theta}\right)\sin\left(k_x x\right). \tag{39}$$

Substitution of Eqs. (33)–(35) into the Fourier transforms of Eqs. (2), (5), (10), and (12) yields the frequency domain expressions of the force and moment resultants of the OCCS:

$$\begin{aligned}\tilde{N}_{\theta\theta}=\frac{C}{R}\sum_{m=1}^{\infty}\sum_{j=1}^{4}\Big[&\left(1-\mu Rk_x\alpha_j+\beta_j\mathrm{i}k_{\theta j}\right)\\&\cdot\left(a_j\mathrm{e}^{\mathrm{i}k_{\theta j}\theta}+d_j\mathrm{e}^{-\mathrm{i}k_{\theta j}\theta}\right)\Big]\sin\left(k_x x\right),\end{aligned} \tag{40}$$

$$\begin{aligned}\tilde{M}_{\theta\theta}=\frac{D}{R^2}\sum_{m=1}^{\infty}\sum_{j=1}^{4}\Big[&\left(k_{\theta j}^2+\mu R^2k_x^2\right)\\&\cdot\left(a_j\mathrm{e}^{\mathrm{i}k_{\theta j}\theta}+d_j\mathrm{e}^{-\mathrm{i}k_{\theta j}\theta}\right)\Big]\sin\left(k_x x\right),\end{aligned} \tag{41}$$

$$\begin{aligned}\tilde{F}_{\theta x}=\frac{1-\mu}{2}\frac{C}{R}\sum_{m=1}^{\infty}\sum_{j=1}^{4}\Big[&\left(\alpha_j\mathrm{i}k_{\theta j}+\beta_jRk_x\right)\\&\cdot\left(a_j\mathrm{e}^{\mathrm{i}k_{\theta j}\theta}-d_j\mathrm{e}^{-\mathrm{i}k_{\theta j}\theta}\right)\Big]\cos\left(k_x x\right),\end{aligned} \tag{42}$$

$$\begin{aligned}\tilde{V}_{\theta z}=\frac{D}{R^3}\sum_{m=1}^{\infty}\sum_{j=1}^{4}\Big\{&\left[(2-\mu)R^2k_x^2\mathrm{i}k_{\theta j}+\mathrm{i}k_{\theta j}^3\right]\\&\cdot\left(a_j\mathrm{e}^{\mathrm{i}k_{\theta j}\theta}-d_j\mathrm{e}^{-\mathrm{i}k_{\theta j}\theta}\right)\Big\}\sin\left(k_x x\right).\end{aligned} \tag{43}$$

2.4 Solutions for OCCS with simply supported straight edges

Since the derivation for solutions of the OCCS with simply supported straight edges is independent of the derivation for the OCCS with simply supported curved edges and the two derivation procedures are quite similar to each other, the symbols used in this subsection will be very similar and frequently the same as those used in the preceding subsection. In addition, the derivation presented in this subsection will be greatly simplified and only the differences between the two derivation procedures will be pointed out.

As the two straight edges of the OCCS are assumed to be simply supported, the boundary conditions at θ=0 and θ=θ_0 are given by (Leissa, 1973)

$$u=0,\ w=0,\ N_{\theta\theta}=0,\ M_{\theta\theta}=0. \tag{44}$$

According to the boundary conditions defined by Eq. (44), the axial, circumferential, and radial displacements of the OCCS can be written as

$$\tilde{u}(x,\theta)=\sum_{n=1}^{\infty}U(x)\sin\left(k_\theta\theta\right), \tag{45}$$

$$\tilde{v}(x,\theta)=\sum_{n=1}^{\infty}V(x)\cos\left(k_\theta\theta\right), \tag{46}$$

$$\tilde{w}(x,\theta)=\sum_{n=1}^{\infty}W(x)\sin\left(k_\theta\theta\right), \tag{47}$$

where k_θ=$n\pi/\theta_0$ denotes the wave number in the circumferential direction, and n is the circumferential mode number.

Assuming that the axial, circumferential, and radial displacements can be expressed by exponential functions of the axial variable x, a common axial wave number equation of the axial, circumferential, and radial displacements of the OCCS can be obtained as

$$\begin{aligned}&\left(k_x^2+\frac{1}{R^2}k_\theta^2-\gamma^2\right)\left(k_x^2+\frac{1}{R^2}k_\theta^2+\gamma^2\right)\\&\times\left(k_x^2+\frac{1}{R^2}k_\theta^2-k_L^2\right)\left(k_x^2+\frac{1}{R^2}k_\theta^2-\frac{2k_L^2}{1-\mu}\right)\\&+\frac{\mu(1-\mu)(2+\mu)}{1+\mu}\frac{1}{R^4\lambda}\left(k_x^2-\frac{1}{\mu R^2}k_\theta^2-\frac{2k_L^2}{1-\mu}\right)\\&\times\left(k_x^2+\frac{1}{2+\mu}\frac{1}{R^2}k_\theta^2-\frac{2k_L^2}{(1-\mu)(2+\mu)}\right)=0.\end{aligned} \tag{48}$$

By solving Eq. (48), eight axial wave numbers are obtained as follows:

$$k_x=\pm k_{x1},\ \pm k_{x2},\ \pm k_{x3},\ \pm k_{x4}. \tag{49}$$

Therefore, for the boundary conditions defined by Eq. (44), the solutions of Eqs. (18)–(20) are written as

$$\tilde{u}(x,\theta)=\sum_{n=1}^{\infty}\sum_{j=1}^{4}\alpha_j'\left(a_j\mathrm{e}^{\mathrm{i}k_{xj}x}-d_j\mathrm{e}^{-\mathrm{i}k_{xj}x}\right)\sin\left(k_\theta\theta\right), \tag{50}$$

$$\tilde{v}(x,\theta)=\sum_{n=1}^{\infty}\sum_{j=1}^{4}\beta_j'\left(a_j\mathrm{e}^{\mathrm{i}k_{xj}x}+d_j\mathrm{e}^{-\mathrm{i}k_{xj}x}\right)\cos\left(k_\theta\theta\right), \tag{51}$$

$$\tilde{w}(x,\theta)=\sum_{n=1}^{\infty}\sum_{j=1}^{4}\left(a_j\mathrm{e}^{\mathrm{i}k_{xj}x}+d_j\mathrm{e}^{-\mathrm{i}k_{xj}x}\right)\sin\left(k_\theta\theta\right), \tag{52}$$

where α'_j and β'_j (j=1, 2, 3, 4) are ratios of the amplitudes of the axial and circumferential waves to the amplitude of the radial wave. The expressions of α'_j and β'_j are defined as follows:

$$\alpha_j'=\frac{\mathrm{i}Rk_{xj}\left(\mu R^2k_{xj}^2-k_\theta^2-\dfrac{2\mu R^2k_L^2}{1-\mu}\right)}{\left(R^2k_{xj}^2+k_\theta^2-R^2k_L^2\right)\left(R^2k_{xj}^2+k_\theta^2-\dfrac{2R^2k_L^2}{1-\mu}\right)}, \tag{53}$$

$$\beta_j'=\frac{k_\theta\left((2+\mu)R^2k_{xj}^2+k_\theta^2-\dfrac{2R^2k_L^2}{1-\mu}\right)}{\left(R^2k_{xj}^2+k_\theta^2-R^2k_L^2\right)\left(R^2k_{xj}^2+k_\theta^2-\dfrac{2R^2k_L^2}{1-\mu}\right)}. \tag{54}$$

The rotation of the normal to the middle surface about the circumferential direction is defined as

$$\phi_x=-\partial w/\partial x. \tag{55}$$

Substituting Eq. (52) into the Fourier transform of Eq. (55) yields the frequency domain expression of the rotation as

$$\tilde{\phi}_x=\sum_{n=1}^{\infty}\sum_{j=1}^{4}-\mathrm{i}k_{xj}\left(a_j\mathrm{e}^{\mathrm{i}k_{xj}x}-d_j\mathrm{e}^{-\mathrm{i}k_{xj}x}\right)\sin\left(k_\theta\theta\right). \quad (56)$$

Substituting Eqs. (50)–(52) into the Fourier transforms of Eqs. (1), (4), (9), and (11) yields the frequency domain expressions of the force and moment resultants of the OCCS:

$$\begin{aligned}\tilde{N}_{xx}=C\sum_{n=1}^{\infty}\sum_{j=1}^{4}\Bigg[&\left(\frac{\mu}{R}+\mathrm{i}k_{xj}\alpha_j'-\frac{\mu k_\theta\beta_j'}{R}\right)\\&\cdot\left(a_j\mathrm{e}^{\mathrm{i}k_{xj}x}+d_j\mathrm{e}^{-\mathrm{i}k_{xj}x}\right)\Bigg]\sin\left(k_\theta\theta\right),\end{aligned} \quad (57)$$

$$\begin{aligned}\tilde{M}_{xx}=D\sum_{n=1}^{\infty}\sum_{j=1}^{4}\Bigg[&\left(k_{xj}^2+\mu\frac{k_\theta^2}{R^2}\right)\\&\cdot\left(a_j\mathrm{e}^{\mathrm{i}k_{xj}x}+d_j\mathrm{e}^{-\mathrm{i}k_{xj}x}\right)\Bigg]\sin\left(k_\theta\theta\right),\end{aligned} \quad (58)$$

$$\begin{aligned}\tilde{F}_{x\theta}=6D\sum_{n=1}^{\infty}\sum_{j=1}^{4}\Bigg[&\left(\frac{\alpha_j'k_\theta}{Rh^2}+\frac{\mathrm{i}k_{xj}\beta_j'}{h^2}-\frac{\mathrm{i}k_{xj}k_\theta}{6R^2}\right)\\&\cdot(1-\mu)\left(a_j\mathrm{e}^{\mathrm{i}k_{xj}x}-d_j\mathrm{e}^{-\mathrm{i}k_{xj}x}\right)\Bigg]\cos\left(k_\theta\theta\right),\end{aligned} \quad (59)$$

$$\begin{aligned}\tilde{V}_{xz}=D\sum_{n=1}^{\infty}\sum_{j=1}^{4}\Bigg\{&\left[(2-\mu)\mathrm{i}k_{xj}\frac{k_\theta^2}{R^2}+\mathrm{i}k_{xj}^3\right]\\&\cdot\left(a_j\mathrm{e}^{\mathrm{i}k_{xj}x}-d_j\mathrm{e}^{-\mathrm{i}k_{xj}x}\right)\Bigg\}\sin\left(k_\theta\theta\right).\end{aligned} \quad (60)$$

2.5 Solutions expressed in matrix form

2.5.1 Simply supported curved edges

For an arbitrary axial mode number m, Eqs. (33)–(35) and (39) can be expressed in matrix form as

$$\boldsymbol{W}_{\mathrm{d}}=\boldsymbol{H}_{\mathrm{m}}(x)\boldsymbol{W}_{\mathrm{d}}^{*}, \quad (61)$$

where $\boldsymbol{W}_{\mathrm{d}}$ denotes the displacement vector of the OCCS, $\boldsymbol{H}_{\mathrm{m}}(x)$ indicates the axial mode matrix, and $\boldsymbol{W}_{\mathrm{d}}^{*}$ represents the wave vector of the circumferential displacement. They are presented in detail as follows:

$$\boldsymbol{W}_{\mathrm{d}}=\left[\tilde{u}\quad\tilde{v}\quad\tilde{w}\quad\tilde{\phi}_\theta\right]^{\mathrm{T}}, \quad (62)$$

$$\boldsymbol{H}_{\mathrm{m}}(x)=\mathrm{diag}\left(\cos(k_x x)\ \ \sin(k_x x)\ \ \sin(k_x x)\ \ \sin(k_x x)\right), \quad (63)$$

$$\boldsymbol{W}_{\mathrm{d}}^{*}=\boldsymbol{A}_{\mathrm{d}}\boldsymbol{P}_{\mathrm{h}}(\theta)\boldsymbol{a}+\boldsymbol{D}_{\mathrm{d}}\boldsymbol{P}_{\mathrm{h}}(-\theta)\boldsymbol{d}, \quad (64)$$

where $\boldsymbol{P}_{\mathrm{h}}(\theta)$ denotes the phase matrix, $\boldsymbol{A}_{\mathrm{d}}$ and $\boldsymbol{D}_{\mathrm{d}}$ are coefficient matrices of fourth-order, $\boldsymbol{a}$ and $\boldsymbol{d}$ are amplitude vectors of the arriving wave and the departing wave corresponding to the displacements of the OCCS, which can be given by

$$\boldsymbol{P}_{\mathrm{h}}(\theta)=\mathrm{diag}\left(\mathrm{e}^{\mathrm{i}k_{\theta 1}\theta}\quad\mathrm{e}^{\mathrm{i}k_{\theta 2}\theta}\quad\mathrm{e}^{\mathrm{i}k_{\theta 3}\theta}\quad\mathrm{e}^{\mathrm{i}k_{\theta 4}\theta}\right), \quad (65)$$

$$\boldsymbol{a}=\left[a_1\quad a_2\quad a_3\quad a_4\right]^{\mathrm{T}}, \quad (66)$$

$$\boldsymbol{d}=\left[d_1\quad d_2\quad d_3\quad d_4\right]^{\mathrm{T}}, \quad (67)$$

$$\begin{cases}\boldsymbol{A}_{\mathrm{d}}(1,j)=\boldsymbol{D}_{\mathrm{d}}(1,j)=\alpha_j,\\ \boldsymbol{A}_{\mathrm{d}}(2,j)=-\boldsymbol{D}_{\mathrm{d}}(2,j)=\beta_j,\\ \boldsymbol{A}_{\mathrm{d}}(3,j)=\boldsymbol{D}_{\mathrm{d}}(3,j)=1,\\ \boldsymbol{A}_{\mathrm{d}}(4,j)=-\boldsymbol{D}_{\mathrm{d}}(4,j)=\left(\beta_j-\mathrm{i}k_{\theta j}\right)/R,\end{cases} \quad (68)$$

where j=1, 2, 3, 4.

Meanwhile, Eqs. (40)–(43) can be expressed in matrix form as

$$\boldsymbol{W}_{\mathrm{f}}=\boldsymbol{H}_{\mathrm{m}}(x)\boldsymbol{W}_{\mathrm{f}}^{*}, \quad (69)$$

where $\boldsymbol{H}_{\mathrm{m}}(x)$ is defined in Eq. (63). $\boldsymbol{W}_{\mathrm{f}}$ denotes the force vector of the shell, and $\boldsymbol{W}_{\mathrm{f}}^{*}$ represents the wave vector of the circumferential force and moment resultants. Then, we can obtain:

$$\boldsymbol{W}_{\mathrm{f}}=\left[\tilde{F}_{\theta x}\quad\tilde{N}_{\theta\theta}\quad\tilde{V}_{\theta z}\quad\tilde{M}_{\theta\theta}\right]^{\mathrm{T}}, \quad (70)$$

$$\boldsymbol{W}_{\mathrm{f}}^{*}=\boldsymbol{A}_{\mathrm{f}}\boldsymbol{P}_{\mathrm{h}}(\theta)\boldsymbol{a}+\boldsymbol{D}_{\mathrm{f}}\boldsymbol{P}_{\mathrm{h}}(-\theta)\boldsymbol{d}, \quad (71)$$

in which the physical significances and expressions of $\boldsymbol{P}_{\mathrm{h}}(\theta)$, $\boldsymbol{a}$, and $\boldsymbol{d}$ are the same as those presented in Eq. (64). However, $\boldsymbol{A}_{\mathrm{f}}$ and $\boldsymbol{D}_{\mathrm{f}}$ are coefficient matrices of the arriving wave and the departing wave corresponding to the force and moment resultants of the OCCS. They are presented as

$$\begin{aligned}&\boldsymbol{A}_{\mathrm{f}}(1,j)=-\boldsymbol{D}_{\mathrm{f}}(1,j)=\frac{(1-\mu)C}{2R}\left(\alpha_j\mathrm{i}k_{\theta j}+\beta_jRk_x\right),\\&\boldsymbol{A}_{\mathrm{f}}(2,j)=\boldsymbol{D}_{\mathrm{f}}(2,j)=\frac{C}{R}\left(-\mu Rk_x\alpha_j+\beta_j\mathrm{i}k_{\theta j}+1\right),\\&\boldsymbol{A}_{\mathrm{f}}(3,j)=-\boldsymbol{D}_{\mathrm{f}}(3,j)=\frac{D}{R^3}\left[(2-\mu)R^2k_x^2\mathrm{i}k_{\theta j}+\mathrm{i}k_{\theta j}^3\right],\\&\boldsymbol{A}_{\mathrm{f}}(4,j)=\boldsymbol{D}_{\mathrm{f}}(4,j)=\frac{D}{R^2}\left(k_{\theta j}^2+\mu R^2k_x^2\right),\end{aligned} \quad (72)$$

where j=1, 2, 3, 4.

2.5.2 Simply supported straight edges

For an arbitrary circumferential mode number n, Eqs. (50)–(52) and (56) can be written in the same matrix form as Eq. (61) only if the element $\tilde{\phi}_\theta$ in $\boldsymbol{W}_\mathrm{d}$ is replaced by $\tilde{\phi}_x$, the axial mode matrix $\boldsymbol{H}_\mathrm{m}(x)$ and the phase matrix $\boldsymbol{P}_\mathrm{h}(\theta)$ are replaced by the circumferential mode matrix $\boldsymbol{H}_\mathrm{n}(\theta)$ and the phase matrix $\boldsymbol{P}_\mathrm{h}(x)$ defined as follows:

$$\boldsymbol{H}_\mathrm{n}(\theta)=\mathrm{diag}\left(\sin(k_\theta\theta)\ \cos(k_\theta\theta)\ \sin(k_\theta\theta)\ \sin(k_\theta\theta)\right), \tag{73}$$

$$\boldsymbol{P}_\mathrm{h}(x)=\mathrm{diag}\left(\mathrm{e}^{\mathrm{i}k_{x1}x}\quad \mathrm{e}^{\mathrm{i}k_{x2}x}\quad \mathrm{e}^{\mathrm{i}k_{x3}x}\quad \mathrm{e}^{\mathrm{i}k_{x4}x}\right). \tag{74}$$

The elements of the coefficient matrices $\boldsymbol{A}_\mathrm{d}$ and $\boldsymbol{D}_\mathrm{d}$ are replaced by

$$\begin{cases}\boldsymbol{A}_\mathrm{d}(1,j)=-\boldsymbol{D}_\mathrm{d}(1,j)=\alpha_j,\\ \boldsymbol{A}_\mathrm{d}(2,j)=\boldsymbol{D}_\mathrm{d}(2,j)=\beta_j,\\ \boldsymbol{A}_\mathrm{d}(3,j)=\boldsymbol{D}_\mathrm{d}(3,j)=1,\\ \boldsymbol{A}_\mathrm{d}(4,j)=-\boldsymbol{D}_\mathrm{d}(4,j)=\mathrm{i}k_{xj},\end{cases} \tag{75}$$

where j=1, 2, 3, 4.

Eqs. (57)–(60) can be written in the same matrix form as Eq. (69) only if the axial mode matrix $\boldsymbol{H}_\mathrm{m}(x)$ and the phase matrix $\boldsymbol{P}_\mathrm{h}(\theta)$ are replaced by the circumferential mode matrix $\boldsymbol{H}_\mathrm{n}(\theta)$ and the phase matrix $\boldsymbol{P}_\mathrm{h}(x)$, and the force vector $\boldsymbol{W}_\mathrm{f}$ turns to be

$$\boldsymbol{W}_\mathrm{f}=\left[\tilde{F}_{x\theta}\quad \tilde{N}_{xx}\quad \tilde{V}_{xz}\quad \tilde{M}_{xx}\right]^\mathrm{T}. \tag{76}$$

The elements of the coefficient matrices $\boldsymbol{A}_\mathrm{f}$ and $\boldsymbol{D}_\mathrm{f}$ are replaced by

$$\begin{aligned}&\boldsymbol{A}_\mathrm{f}(1,j)=\boldsymbol{D}_\mathrm{f}(1,j)=C\left(\mathrm{i}k_{xj}\alpha_j+\frac{\mu-\mu k_\theta\beta_j}{R}\right),\\ &\boldsymbol{A}_\mathrm{f}(2,j)=-\boldsymbol{D}_\mathrm{f}(2,j)\\ &\qquad=6(1-\mu)D\left(\frac{\alpha_j k_\theta+\mathrm{i}Rk_{xj}\beta_j}{Rh^2}-\frac{\mathrm{i}k_{xj}k_\theta}{6R^2}\right),\\ &\boldsymbol{A}_\mathrm{f}(3,j)=-\boldsymbol{D}_\mathrm{f}(3,j)=D\left[(2-\mu)\frac{\mathrm{i}k_{xj}k_\theta^2}{R^2}+\mathrm{i}k_{xj}^3\right],\\ &\boldsymbol{A}_\mathrm{f}(4,j)=\boldsymbol{D}_\mathrm{f}(4,j)=D\left(k_{xj}^2+\mu\frac{k_\theta^2}{R^2}\right),\end{aligned} \tag{77}$$

where j=1, 2, 3, 4.

2.6 Equations of natural frequencies

Taking advantage of the unidirectional traveling wave solutions of the OCCS with simply supported curved edges and simply supported straight edges which are respectively obtained in Subsections 2.3 and 2.4, the MRRM is introduced to derive the equation of natural frequencies of the OCCS. Since the scattering matrix is related to boundary conditions of the remaining two edges, it will be discussed in the first step. Then, the phase matrix and permutation matrix, which are independent of the boundary conditions, are obtained. Finally, the reverberation matrix and the equation for natural frequencies of the OCCS are derived. The formulations mentioned above are presented in detail in the following discussion.

Since the derivation procedures of the scattering matrix, phase matrix, and permutation matrix for the OCCS with simply supported curved edges and simply supported straight edges are very similar to each other, the one for simply supported curved edges will be taken as an example and the other will be omitted. Note that the only difference between the two derivation procedures is that the one for simply supported curved edges takes advantage of the solutions obtained in Section 2.3 while the other one employs the solutions obtained in Section 2.4.

2.6.1 Scattering matrix for various classical boundary conditions

With regard to an OCCS with simply supported curved edges and simply supported straight edges, the boundary conditions and the dual local coordinate systems of the OCCS are shown in Fig. 3. The scattering matrix corresponding to various classical boundary conditions, including simply supported edges, free edges, and clamped edges, of the remaining two edges are derived in the following discussion.

1. Simply supported edge

Assuming that the OCCS is simply supported at Node Line 1, the boundary conditions are defined in the local coordinate $(ox\theta z)^{12}$ as

$$u^{12}=0,\ w^{12}=0,\ N_{\theta\theta}^{12}=0,\ M_{\theta\theta}^{12}=0. \tag{78}$$

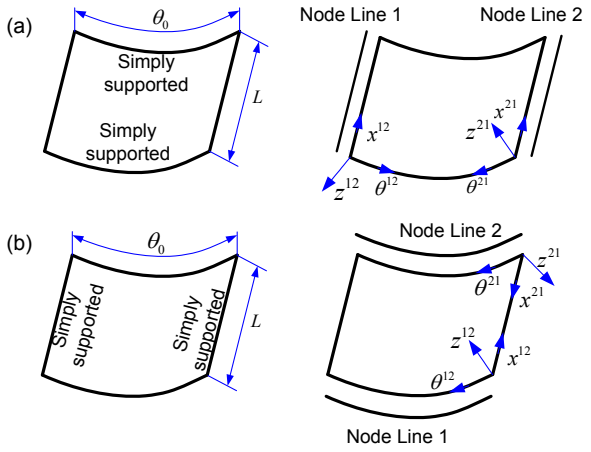

Fig. 3 Boundary conditions and dual local coordinate system of the shell

(a) Simply supported curved edges; (b) Simply supported straight edges

Substitution of Eqs. (33), (35), (40), and (41) into the Fourier transform of Eq. (78) yields

$$\sum_{j=1}^{4}\alpha_j a_j^{12}+\alpha_j d_j^{12}=0, \tag{79}$$

$$\sum_{j=1}^{4}a_j^{12}+d_j^{12}=0, \tag{80}$$

$$\sum_{j=1}^{4}\left[\left(-\mu R k_x\alpha_j+\beta_j \mathrm{i}k_{\theta j}+1\right)a_j^{12}+\left(-\mu R k_x\alpha_j+\beta_j \mathrm{i}k_{\theta j}+1\right)d_j^{12}\right]=0, \tag{81}$$

$$\sum_{j=1}^{4}\left[\left(k_{\theta j}^2+\mu R^2k_x^2\right)a_j^{12}+\left(k_{\theta j}^2+\mu R^2k_x^2\right)d_j^{12}\right]=0. \tag{82}$$

Eqs. (79)–(82) can be presented in matrix form as

$$\boldsymbol{d}^1=\boldsymbol{S}^1\boldsymbol{a}^1, \tag{83}$$

where $\boldsymbol{d}^1=\boldsymbol{d}^{12}=[d_1^{12}\ d_2^{12}\ d_3^{12}\ d_4^{12}]^{\mathrm{T}}$ and $\boldsymbol{a}^1=\boldsymbol{a}^{12}=[a_1^{12}\ a_2^{12}\ a_3^{12}\ a_4^{12}]^{\mathrm{T}}$ are amplitude vectors of the departing wave and the arriving wave, and $\boldsymbol{S}^1=-\boldsymbol{I}_4$ is defined as the scattering matrix at Node Line 1, in which $\boldsymbol{I}_4$ is a unit matrix of fourth-order.

2. Free edge

Assuming that the edge of the OCCS at Node Line 1 is free, the boundary conditions are defined in the local coordinate $(ox\theta z)^{12}$ as

$$N_{\theta\theta}^{12}=0,\ \ F_{\theta x}^{12}=0,\ \ V_{\theta z}^{12}=0,\ \ M_{\theta\theta}^{12}=0. \tag{84}$$

Substitution of Eq. (69) into the Fourier transform of Eq. (84) yields

$$\boldsymbol{W}_{\mathrm{f}}^{*12}=\boldsymbol{A}_{\mathrm{f}}\boldsymbol{P}_{\mathrm{h}}(0)\boldsymbol{a}^{12}+\boldsymbol{D}_{\mathrm{f}}\boldsymbol{P}_{\mathrm{h}}(0)\boldsymbol{d}^{12}=\boldsymbol{0}. \tag{85}$$

Since the phase matrix turns into a unit matrix at the origin of the local coordinate, which is obvious from its definition, Eq. (85) can be presented in the same form as Eq. (83) with the scattering matrix replaced by $\boldsymbol{S}^1=-\boldsymbol{D}_{\mathrm{f}}^{-1}\boldsymbol{A}_{\mathrm{f}}$.

3. Clamped edge

Assuming that the edge of the OCCS at Node Line 1 is clamped, the boundary conditions are defined in the local coordinate $(ox\theta z)^{12}$ as

$$u^{12}=0,\ \ v^{12}=0,\ \ w^{12}=0,\ \ \phi_\theta^{12}=0. \tag{86}$$

Substituting Eq. (61) into the Fourier transform of Eq. (86) yields

$$\boldsymbol{W}_{\mathrm{d}}^{*12}=\boldsymbol{A}_{\mathrm{d}}\boldsymbol{P}_{\mathrm{h}}(0)\boldsymbol{a}^{12}+\boldsymbol{D}_{\mathrm{d}}\boldsymbol{P}_{\mathrm{h}}(0)\boldsymbol{d}^{12}=\boldsymbol{0}. \tag{87}$$

In a same manner, Eq. (87) can be presented in the same form as Eq. (83) with the scattering matrix replaced by $\boldsymbol{S}^1=-\boldsymbol{D}_{\mathrm{d}}^{-1}\boldsymbol{A}_{\mathrm{d}}$.

Similarly, the scattering relation for the OCCS at Node Line 2 is presented as

$$\boldsymbol{d}^2=\boldsymbol{S}^2\boldsymbol{a}^2, \tag{88}$$

where $\boldsymbol{d}^2=\boldsymbol{d}^{21}=[d_1^{21}\ d_2^{21}\ d_3^{21}\ d_4^{21}]^{\mathrm{T}}$ and $\boldsymbol{a}^2=\boldsymbol{a}^{21}=[a_1^{21}\ a_2^{21}\ a_3^{21}\ a_4^{21}]^{\mathrm{T}}$ are amplitude vectors of the departing wave and the arriving wave at Node Line 2. In the same manner as the scattering matrix for Node Line 1 is derived, the scattering matrix at Node Line 2 can be obtained as $\boldsymbol{S}^2=-\boldsymbol{I}_4$ for a simply supported edge, $\boldsymbol{S}^2=-\boldsymbol{D}_{\mathrm{f}}^{-1}\boldsymbol{A}_{\mathrm{f}}$ for a free edge, and $\boldsymbol{S}^2=-\boldsymbol{D}_{\mathrm{d}}^{-1}\boldsymbol{A}_{\mathrm{d}}$ for a clamped edge.

Assembling both of the local scattering equations at Node Line 1 and Node Line 2 by stacking $\boldsymbol{d}^1$ and $\boldsymbol{d}^2$, $\boldsymbol{a}^1$ and $\boldsymbol{a}^2$ into two column vectors $\boldsymbol{d}$ and $\boldsymbol{a}$, the global scattering equation is obtained:

$$\boldsymbol{d}=\boldsymbol{S}\boldsymbol{a}, \tag{89}$$

where $\boldsymbol{d}=[(\boldsymbol{d}^1)^{\mathrm{T}}\ (\boldsymbol{d}^2)^{\mathrm{T}}]^{\mathrm{T}}$ and $\boldsymbol{a}=[(\boldsymbol{a}^1)^{\mathrm{T}}\ (\boldsymbol{a}^2)^{\mathrm{T}}]^{\mathrm{T}}$ are global amplitude vectors of the departing wave and the arriving wave, and $\boldsymbol{S}=\mathrm{diag}(\boldsymbol{S}^1\ \boldsymbol{S}^2)$ is the global scattering matrix.

2.6.2 Phase and permutation matrices

The phase relations of harmonic waves in the dual coordinate system of MRRM provide additional equations for solving the unknown amplitude vectors. Note that the departing wave from Node Line 1 is exactly the arriving wave to Node Line 2, and vice versa. Therefore, the amplitudes of the departing wave and the arriving wave differ with each other by a phase factor.

With the employment of the solutions of the OCCS with simply supported curved edges, the relations between the amplitudes of the departing wave and the arriving wave are presented as

$$\begin{cases} a_1^{12}=-\mathrm{e}^{-\mathrm{i}k_{\theta 1}\theta_0}d_1^{21},\ a_2^{12}=-\mathrm{e}^{-\mathrm{i}k_{\theta 2}\theta_0}d_2^{21}, \\ a_3^{12}=-\mathrm{e}^{-\mathrm{i}k_{\theta 3}\theta_0}d_3^{21},\ a_4^{12}=-\mathrm{e}^{-\mathrm{i}k_{\theta 4}\theta_0}d_4^{21}, \end{cases} \tag{90}$$

$$\begin{cases} a_1^{21}=-\mathrm{e}^{-\mathrm{i}k_{\theta 1}\theta_0}d_1^{12},\ a_2^{21}=-\mathrm{e}^{-\mathrm{i}k_{\theta 2}\theta_0}d_2^{12}, \\ a_3^{21}=-\mathrm{e}^{-\mathrm{i}k_{\theta 3}\theta_0}d_3^{12},\ a_4^{21}=-\mathrm{e}^{-\mathrm{i}k_{\theta 4}\theta_0}d_4^{12}, \end{cases} \tag{91}$$

which are rewritten in matrix form as

$$\boldsymbol{a}^1=-\boldsymbol{P}_{\mathrm{h}}(-\theta_0)\boldsymbol{d}^2, \tag{92}$$

$$\boldsymbol{a}^2=-\boldsymbol{P}_{\mathrm{h}}(-\theta_0)\boldsymbol{d}^1. \tag{93}$$

Assembling both the local phase equations defined by Eqs. (92) and (93) results in the global phase equation

$$\boldsymbol{a}=\boldsymbol{P}\boldsymbol{d}^*, \tag{94}$$

where $\boldsymbol{a}$ is defined in Eq. (89). However, $\boldsymbol{d}^*=[(\boldsymbol{d}^2)^{\mathrm{T}}\ (\boldsymbol{d}^1)^{\mathrm{T}}]^{\mathrm{T}}$ is a rearranged global amplitude vector of the departing wave, and $\boldsymbol{P}=-\mathrm{diag}(\boldsymbol{P}_{\mathrm{h}}(-\theta_0)\ \boldsymbol{P}_{\mathrm{h}}(-\theta_0))$ is the global phase matrix.

A comparison of the global amplitude vectors of the departing waves $\boldsymbol{d}$ and $\boldsymbol{d}^*$ indicates that the two amplitude vectors contain the same scalar state variables arranged in different sequential orders. The relation between $\boldsymbol{d}$ and $\boldsymbol{d}^*$ is

$$\boldsymbol{d}^*=\boldsymbol{U}\boldsymbol{d}, \tag{95}$$

where $\boldsymbol{U}=[\boldsymbol{0}_4\ \boldsymbol{I}_4;\ \boldsymbol{I}_4\ \boldsymbol{0}_4]$ is the permutation matrix from $\boldsymbol{d}$ to $\boldsymbol{d}^*$, in which $\boldsymbol{0}_4$ and $\boldsymbol{I}_4$ are respectively the zero matrix and the unit matrix of fourth-order.

2.6.3 Equation for natural frequencies

Substitution of Eqs. (94) and (95) into Eq. (89) yields

$$(\boldsymbol{I}-\boldsymbol{R})\boldsymbol{d}=\boldsymbol{0}, \tag{96}$$

where $\boldsymbol{R}=\boldsymbol{SPU}$ is defined as the reverberation-ray matrix.

To obtain a nontrivial solution of the global amplitude vector of the departing wave $\boldsymbol{d}$, the determinant of $(\boldsymbol{I}-\boldsymbol{R})$ must be zero:

$$\det(\boldsymbol{I}-\boldsymbol{R})=0, \tag{97}$$

which is the equation of natural frequencies of the OCCS.

2.7 Searching algorithm for natural frequencies

As the equation of natural frequencies of the OCCS is obtained, the problem at hand is to solve the equation for the natural frequencies. It is obvious that the left hand side of Eq. (97) represents a function of frequency, and the natural frequencies are zero points of the function. Unfortunately, for most values of the frequency, the left hand side of Eq. (97) are complex numbers. Therefore, finding the zero points of the function needs to search the common zero points of the real part and the imaginary part of the function. A good idea is to search the zero points or the minimal values of the absolute value of the function. This simple approach is adopted in this paper and the golden section search algorithm (GSSA) (Press *et al.*, 1992; Vajda, 2007) is introduced to determine the natural frequencies of the OCCS. The procedure for determining natural frequencies of the OCCS, which is shown in Fig. 4, is presented in detail as follows.

Firstly, for a trial value of frequency ω_1 and a given frequency step $\Delta\omega$, choose both of the endpoints of the interval (ω_1, $\omega_1+\Delta\omega$) and the points with the distance of golden ratio of the interval length from the endpoints as observation frequencies and calculate the absolute values of the determinant of $(\boldsymbol{I}-\boldsymbol{R})$ for the observation frequencies.

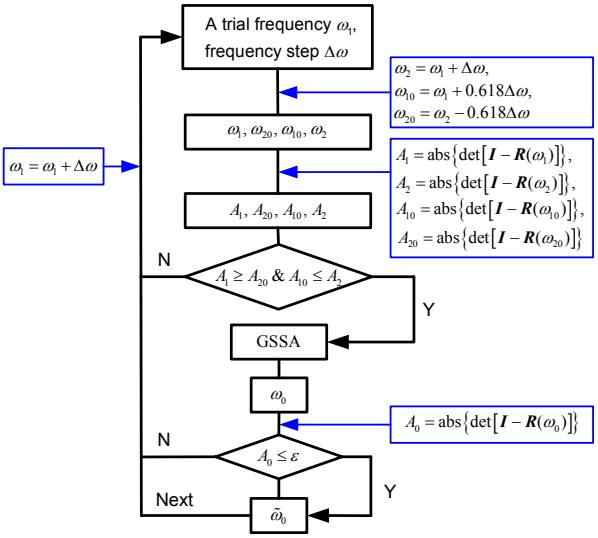

Fig. 4 Calculation procedure for natural frequencies of the OCCS (Guo, 2008)

Secondly, compare the absolute values of the determinant for the two frequencies at the left hand side and for the two frequencies at the right hand side of the interval to determine whether there is a zero point or minimal value in the interval. If the answer is yes, the golden section search algorithm is employed to find the zero point or minimal value; if not, the trial frequency will increase by a frequency step, and the above-mentioned process will be repeated until the answer becomes yes.

Thirdly, calculate the absolute value of the determinant for the minimal value obtained in the preceding step to check whether the calculation result is less than the predefined tolerance. If the answer is no, the minimal value will be ignored and the trial frequency will increase by a frequency step, and the above-mentioned process will be repeated until the answer becomes yes. While if the answer is yes, the minimal value is one of the natural frequencies and then the trial frequency will increase by a frequency step, and the above-mentioned process will be repeated to find the next natural frequency. The procedure will be terminated when enough natural frequencies are obtained.

2.8 Mode shapes for the OCCS

Substituting one of the natural frequencies determined in the preceding subsection into Eq. (96), the global amplitude vector of the departing wave $\boldsymbol{d}$ is obtained. By normalization, the global amplitude vector of the departing wave is determinate. Subsequently, by substituting the global amplitude vector of the departing wave into Eqs. (94) and (95), the global amplitude vector of the arriving wave $\boldsymbol{a}$ is determined.

Finally, substituting the global amplitude vector of the departing wave and the arriving wave into the expressions of the displacement components of the OCCS, the mode shape corresponding to the natural frequency is obtained.

3 Results and discussion

The MRRM and the golden section search algorithm are applied in this section to obtain the exact natural frequencies for the OCCS. To begin with, the natural frequencies for the OCCS with all four edges simply supported are calculated and compared with the results obtained by FEM and the method of Leissa. Then, natural frequencies for the OCCS of different length, radius, thickness, and included angle are obtained and the effects of these parameters on the natural frequencies are analyzed. Finally, natural frequencies for the OCCS with different boundary conditions are calculated and the effects of boundary conditions on the natural frequencies are also analyzed.

3.1 Verification of the method

The basic parameters of the OCCS are defined in Table 1. For such an OCCS with all four edges simply supported, a comparison study, with the calculation results shown in Table 2, is carried out by the MRRM presented in this paper, FEM, and the method of Leissa. In addition, some mode shapes obtained by FEM and MRRM are presented in Fig. 5.

Table 1 Basic parameters of the OCCS

Parameter	Value	Parameter	Value
E (Pa)	2.1×10^{11}	R (m)	5
μ	0.3	L (m)	10
ρ (kg/m^3)	7800	θ_0	30°
h (mm)	6		

Table 2 Comparison of natural frequencies obtained by FEM, Leissa's method (LM), and MRRM

n	Method	f (Hz)									
		m=1	m=2	m=3	m=4	m=5	m=6	m=7	m=8	m=9	m=10
1	FEM	10.704	34.971	62.339	85.755	103.823	117.321	127.288	134.768	140.495	144.995
	LM	10.683442	35.112306	62.316851	85.708706	103.795915	117.260737	127.239727	134.726258	140.462083	144.974008
	MRRM1	10.683442	35.112306	62.316851	85.708706	103.795915	117.260737	127.239727	134.726258	140.462083	144.974008
	MRRM2	10.683442	35.112306	62.316851	85.708706	103.795915	117.260737	127.239727	134.726258	140.462083	144.974008
2	FEM	9.245	14.052	24.183	37.104	50.937	64.442	76.948	88.190	98.172	106.914
	LM	9.182095	13.997569	24.121208	37.061445	50.864659	64.336077	76.826046	88.060313	97.997932	106.725825
	MRRM1	9.182095	13.997569	24.121208	37.061445	50.864659	64.336077	76.826046	88.060313	97.997932	106.725825
	MRRM2	9.182095	13.997569	24.121208	37.061445	50.864659	64.336077	76.826046	88.060313	97.997932	106.725825
3	FEM	19.712	20.693	23.368	28.291	35.164	43.364	52.293	61.447	70.528	79.351
	LM	19.589616	20.577955	23.272018	28.184010	35.052102	43.239370	52.131339	61.261467	70.311352	79.082207
	MRRM1	19.589616	20.577955	23.272018	28.184010	35.052102	43.239370	52.131339	61.261467	70.311352	79.082207
	MRRM2	19.589616	20.577955	23.272018	28.184010	35.052102	43.239370	52.131339	61.261467	70.311352	79.082207
4	FEM	34.895	35.585	36.585	38.599	41.626	45.754	50.850	56.766	63.268	70.165
	LM	34.671416	35.217166	36.365375	38.368545	41.409543	45.529062	50.627393	56.518955	62.993151	69.855024
	MRRM1	34.671416	35.217166	36.365375	38.368545	41.409543	45.529062	50.627393	56.518955	62.993151	69.855024
	MRRM2	34.671416	35.217166	36.365375	38.368545	41.409543	45.529062	50.627393	56.518955	62.993151	69.855024
5	FEM	54.536	55.015	55.846	57.172	59.042	61.516	64.666	68.463	72.878	77.822
	LM	54.098700	54.569540	55.421826	56.739317	58.608406	61.096957	64.239020	68.029361	72.427699	77.369168
	MRRM1	54.098700	54.569540	55.421826	56.739317	58.608406	61.096957	64.239020	68.029361	72.427699	77.369168
	MRRM2	54.098700	54.569540	55.421826	56.739317	58.608406	61.096957	64.239020	68.029361	72.427699	77.369168
6	FEM	78.672	79.141	79.922	81.022	82.561	84.511	86.917	89.811	93.149	96.988
	LM	77.848269	78.301104	79.079317	80.213978	81.741024	83.695373	86.105431	88.988979	92.351044	96.183863
	MRRM1	77.848269	78.301104	79.079317	80.213978	81.741024	83.695373	86.105431	88.988979	92.351044	96.183863
	MRRM2	77.848269	78.301104	79.079317	80.213978	81.741024	83.695373	86.105431	88.988979	92.351044	96.183863
7	FEM	107.366	107.859	108.614	109.685	111.097	112.822	114.959	117.468	120.370	123.670
	LM	105.917005	106.364359	107.119472	108.195392	109.608088	111.374545	113.510793	116.030143	118.941828	122.250189
	MRRM1	105.917005	106.364359	107.119472	108.195392	109.608088	111.374545	113.510793	116.030143	118.941828	122.250189
	MRRM2	105.917005	106.364359	107.119472	108.195392	109.608088	111.374545	113.510793	116.030143	118.941828	122.250189
8	FEM	140.590	141.252	142.001	143.047	144.404	146.082	148.089	150.436	153.129	156.174
	LM	138.304293	138.749680	139.496327	140.550307	141.919306	143.611918	145.636879	148.002310	150.715052	153.780149
	MRRM1	138.304293	138.749680	139.496327	140.550307	141.919306	143.611918	145.636879	148.002310	150.715052	153.780149
	MRRM2	138.304293	138.749680	139.496327	140.550307	141.919306	143.611918	145.636879	148.002310	150.715052	153.780149
9	FEM	179.384	179.427	180.181	181.217	182.552	184.192	186.144	188.414	191.006	193.925
	LM	175.009975	175.454567	176.197714	177.242486	178.592856	180.253411	182.229022	184.524509	187.144318	190.092241
	MRRM1	175.009975	175.454567	176.197714	177.242486	178.592856	180.253411	182.229022	184.524509	187.144318	190.092241
	MRRM2	175.009975	175.454567	176.197714	177.242486	178.592856	180.253411	182.229022	184.524509	187.144318	190.092241
10	FEM	222.285	222.501	223.277	224.310	225.633	227.254	229.176	231.405	233.942	236.792
	LM	216.034005	216.478246	217.219805	218.260343	219.602041	221.247476	223.199463	225.460902	228.034611	230.923182
	MRRM1	216.034005	216.478246	217.219805	218.260343	219.602041	221.247476	223.199463	225.460902	228.034611	230.923182
	MRRM2	216.034005	216.478246	217.219805	218.260343	219.602041	221.247476	223.199463	225.460902	228.034611	230.923182

The results by FEM in Table 2 and Fig. 5 are obtained with the common program software ANSYS, in which the geometry and material properties of the open circular cylindrical shell are defined according to Table 1 and a 250×66 finite element mesh (element edge length 0.04 m) of SHELL181

elements is used during the calculation.

The integer numbers m and n in Table 2 denote the half-wave numbers of the vibration mode in the axial and circumferential directions. MRRM1 and MRRM2 represent the results calculated by MRRM with the solutions for simply supported curved edges derived in Section 2.3 and with the solutions for simply supported straight edges derived in Section 2.4.

It is observed from Table 2 that an excellent agreement is achieved between the results obtained by MRRM based on both of the two solutions and the results obtained by the method of Leissa. Therefore, the comparison study confirms the validity of MRRM for vibration analysis of OCCSs. The results obtained by FEM are quite close to those obtained by MRRM.

Fig. 5 shows that the mode shapes obtained by FEM and MRRM are almost the same as each other, which further indicates that MRRM is suitable for free vibration analysis of OCCSs.

Table 2 also shows that the natural frequencies of the OCCS increase with the increase of the axial mode number. However, as the circumferential mode number increases, the natural frequencies of the OCCS firstly decrease to a minimal value at a certain mode number, for example n=2 for m=1, 2, n=3 for m=3–6, and n=4 for m=7–10, and then gradually increase all the way up. Table 2 also shows that the natural frequencies of the OCCS increase with the increase of the circumferential mode number more rapidly than they do with the increase of the axial mode number.

3.2 Effect of shell length on natural frequencies

The effect of shell length on natural frequencies of the OCCS with all four edges simply supported is investigated in this subsection. The shell length is set to be 6 m, 8 m, 10 m, and 12 m, respectively. The other parameters of the OCCS are defined in Table 1. The comparison results are presented in Table 3, in which all the natural frequencies are normalized by the results presented in Table 2. Since all the normalized natural frequencies corresponding to shell length of 10 m turn out to be unit one, they are omitted in this table. The same manner is used for Table 4–8, and it will not be mentioned in the next subsections.

Table 3 shows that, for an arbitrary pair of mode numbers, the natural frequencies of the OCCS decrease with the increase of the shell length.

For an arbitrary axial mode number, the difference of natural frequencies corresponding to different shell lengths decreases with the increase of the circumferential mode number. However, for an arbitrary circumferential mode number, the difference of natural frequencies corresponding to different shell lengths increases with the increase of the axial mode

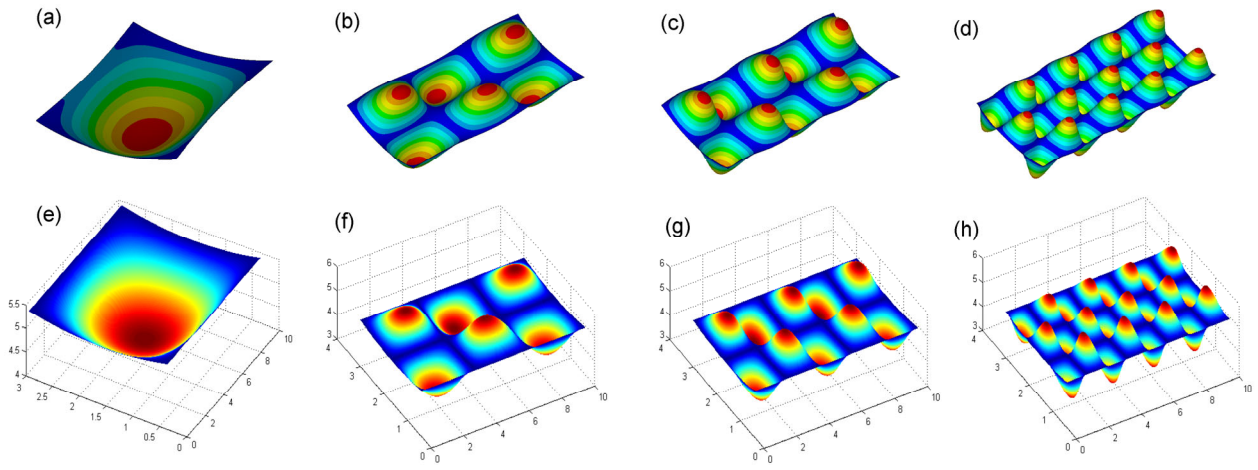

Fig. 5 Comparison of some selected mode shapes calculated by FEM and MRRM
(a) FEM, (m, n)=(1, 1); (b) FEM, (m, n)=(3, 2); (c) FEM, (m, n)=(5, 2); (d) FEM, (m, n)=(8, 3); (e) MRRM, (m, n)=(1, 1); (f) MRRM, (m, n)=(3, 2); (g) MRRM, (m, n)=(5, 2); (h) MRRM, (m, n)=(8, 3)

number, which indicates that the effect of shell length on natural frequencies of the OCCS increases with axial mode number while it decreases with the circumferential mode number.

3.3 Effect of shell radius on natural frequencies

The effects of shell radius on natural frequencies of the OCCS with all four edges simply supported are investigated in this subsection. The shell radii are taken as 3 m, 4 m, 5 m, and 6 m. The other parameters of the OCCS are defined in Table 1. The calculation results are presented in Table 4.

It can be found from Table 4 that, for most but not all of the mode numbers (except for (m, n)= (1–5, 1) and (4–9, 2)), the natural frequencies of the OCCS decrease with the increase of the shell radius. The effect of shell radius on natural frequencies of the OCCS decreases with axial mode number while it increases with circumferential mode number.

Table 3 Effect of shell length on the normalized natural frequencies

n	L (m)	f									
		m=1	m=2	m=3	m=4	m=5	m=6	m=7	m=8	m=9	m=10
1	6	2.446645	2.013127	1.665616	1.449494	1.317999	1.236339	1.184627	1.151977	1.132400	1.122560
	8	1.489498	1.393654	1.289484	1.211031	1.156493	1.119236	1.093686	1.076063	1.063967	1.055900
	12	0.723040	0.744428	0.785251	0.824718	0.858290	0.885172	0.906077	0.922123	0.934362	0.943637
2	6	1.275481	2.017254	2.108711	1.964163	1.799176	1.658880	1.548817	1.465509	1.404142	1.360527
	8	1.069796	1.325123	1.396452	1.372441	1.328358	1.283988	1.244783	1.211963	1.185320	1.164205
	12	0.971580	0.836687	0.768971	0.761888	0.773472	0.790609	0.808931	0.826646	0.842944	0.857472
3	6	1.026277	1.198463	1.506191	1.742872	1.834383	1.828940	1.780379	1.719556	1.660960	1.610634
	8	1.007084	1.052629	1.149522	1.243688	1.295707	1.311067	1.305722	1.290896	1.272818	1.254710
	12	0.996659	0.976986	0.930772	0.875032	0.833283	0.810652	0.802031	0.801827	0.806267	0.813065
4	6	1.008919	1.048541	1.138708	1.272647	1.415676	1.534295	1.614428	1.658727	1.676978	1.679375
	8	1.002689	1.013705	1.038776	1.079258	1.128198	1.174792	1.211422	1.235957	1.249922	1.256120
	12	0.998592	0.993284	0.981698	0.962420	0.936988	0.909519	0.884312	0.863951	0.849095	0.839202
5	6	1.005086	1.022638	1.057497	1.112431	1.184655	1.266334	1.348105	1.422505	1.485494	1.536214
	8	1.001586	1.006845	1.016954	1.032942	1.054810	1.081150	1.109518	1.137291	1.162425	1.183796
	12	0.999147	0.996414	0.991362	0.983531	0.972734	0.959269	0.943932	0.927814	0.912012	0.897395
6	6	1.003430	1.014241	1.033659	1.062784	1.101731	1.149214	1.202747	1.259284	1.315920	1.370376
	8	1.001080	1.004427	1.010314	1.019037	1.030746	1.045307	1.062255	1.080851	1.100230	1.119546
	12	0.999416	0.997627	0.994543	0.990054	0.984087	0.976649	0.967868	0.957985	0.947335	0.936297
7	6	1.002498	1.010129	1.023232	1.042158	1.067045	1.097649	1.133296	1.172954	1.215396	1.259374
	8	1.000789	1.003181	1.007244	1.013057	1.020667	1.030055	1.041106	1.053607	1.067260	1.081713
	12	0.999572	0.998282	0.996109	0.993034	0.989042	0.984139	0.978364	0.971788	0.964521	0.956700
8	6	1.001907	1.007665	1.017369	1.031121	1.048960	1.070804	1.096415	1.125403	1.157246	1.191348
	8	1.000603	1.002417	1.005457	1.009740	1.015272	1.022036	1.029986	1.039039	1.049074	1.059941
	12	0.999673	0.998690	0.997051	0.994755	0.991806	0.988214	0.984002	0.979204	0.973868	0.968055
9	6	1.001505	1.006028	1.013593	1.024219	1.037900	1.054583	1.074154	1.096428	1.121156	1.148037
	8	1.000476	1.001904	1.004286	1.007619	1.011897	1.017104	1.023211	1.030173	1.037931	1.046408
	12	0.999742	0.998967	0.997678	0.995880	0.993580	0.990788	0.987521	0.983800	0.979653	0.975114
10	6	1.001218	1.004874	1.010967	1.019491	1.030427	1.043733	1.059335	1.077130	1.096980	1.118715
	8	1.000385	1.001541	1.003463	1.006147	1.009584	1.013758	1.018648	1.024227	1.030458	1.037296
	12	0.999791	0.999164	0.998122	0.996669	0.994813	0.992563	0.989931	0.986932	0.983585	0.979910

Table 4 Effect of shell radius on the normalized natural frequencies

n	R (m)	f									
		m=1	m=2	m=3	m=4	m=5	m=6	m=7	m=8	m=9	m=10
1	3	0.834182	0.717963	0.799013	0.901277	1.003349	1.096833	1.178429	1.247630	1.305318	1.352900
	4	0.863821	0.871513	0.927372	0.983799	1.032973	1.073129	1.104913	1.129740	1.149053	1.164064
	6	1.150122	1.095293	1.029006	0.977504	0.940855	0.915305	0.897392	0.884657	0.875480	0.868818
2	3	2.626110	1.812428	1.204825	0.971491	0.901613	0.897741	0.922262	0.959452	1.001888	1.045665
	4	1.500395	1.177597	0.980631	0.931605	0.932930	0.950797	0.974075	0.998405	1.021851	1.043522
	6	0.757714	0.997116	1.076325	1.071229	1.046475	1.018935	0.993429	0.971283	0.952621	0.937144
3	3	2.759039	2.651723	2.389903	2.037619	1.718029	1.483523	1.328362	1.231819	1.175411	1.145805
	4	1.555939	1.514070	1.409740	1.274385	1.161459	1.088668	1.048678	1.030192	1.024757	1.034343
	6	0.699488	0.738802	0.828148	0.919363	0.975305	0.999000	1.003476	0.998168	0.988423	0.977086
4	3	2.769661	2.739711	2.675109	2.566300	2.417161	2.245269	2.072229	1.914256	1.779337	1.669104
	4	1.559867	1.549493	1.525738	1.484511	1.427787	1.363514	1.301034	1.246836	1.203535	1.162635
	6	0.696028	0.703713	0.723562	0.758081	0.801947	0.845603	0.881757	0.907810	0.924485	0.933811
5	3	2.772829	2.757095	2.728308	2.683906	2.622421	2.544574	2.453527	2.354189	2.252001	2.151818
	4	1.560923	1.555788	1.546060	1.530560	1.508595	1.480447	1.447471	1.411773	1.375641	1.341049
	6	0.695327	0.698481	0.705151	0.716597	0.733251	0.754263	0.777719	0.801355	0.823261	0.842247
6	3	2.774380	2.764015	2.746228	2.720456	2.686262	2.643568	2.592827	2.535053	2.471746	2.404697
	4	1.561422	1.558106	1.552326	1.543800	1.532288	1.517706	1.500199	1.480159	1.458189	1.435016
	6	0.695036	0.696925	0.700410	0.705859	0.713548	0.723528	0.735559	0.749135	0.763584	0.778206
7	3	2.775289	2.767792	2.755203	2.737424	2.714390	2.686128	2.652802	2.614741	2.572446	2.526566
	4	1.561712	1.559329	1.555300	1.549560	1.542052	1.532751	1.521690	1.508974	1.494779	1.479347
	6	0.694874	0.696195	0.698488	0.701863	0.706420	0.712211	0.719216	0.727328	0.736362	0.746072
8	3	2.775874	2.770163	2.760644	2.747326	2.730241	2.709456	2.685090	2.657319	2.626385	2.592593
	4	1.561897	1.560087	1.557059	1.552804	1.547318	1.540608	1.532699	1.523641	1.513509	1.502407
	6	0.694772	0.695765	0.697447	0.699851	0.703008	0.706940	0.711644	0.717090	0.723219	0.729941
9	3	2.776274	2.771769	2.764279	2.753833	2.740480	2.724287	2.705346	2.683778	2.659732	2.633386
	4	1.562024	1.560597	1.558221	1.554900	1.550642	1.545464	1.539387	1.532445	1.524683	1.516158
	6	0.694703	0.695482	0.696787	0.698629	0.701014	0.703949	0.707427	0.711437	0.715950	0.720929
10	3	2.776560	2.772912	2.766852	2.758409	2.747625	2.734557	2.719277	2.701871	2.682443	2.661113
	4	1.562115	1.560960	1.559040	1.556361	1.552935	1.548775	1.543902	1.538341	1.532121	1.525280
	6	0.694654	0.695283	0.696332	0.697804	0.699698	0.702012	0.704742	0.707877	0.711402	0.715296

3.4 Effect of shell thickness on natural frequencies

Table 5 presents the natural frequencies of the OCCS with all four edges simply supported as the shell thickness varies from 4 mm, by every 2 mm, to 10 mm. The rest parameters of the OCCS are defined in Table 1. The calculation results are presented in Table 5.

It is observed from Table 5 that the natural frequencies of the OCCS increase with the increase of the shell thickness for all mode numbers. The effect of shell thickness on natural frequencies of the OCCS decreases with axial mode number while it increases with the circumferential mode number.

For small circumferential mode numbers n=1 and 2, the natural frequencies corresponding to different shell thickness are very close to each other. However, for large circumferential mode numbers n ≥7, the natural frequencies vary linearly with the shell thickness.

Table 5 Effect of shell thickness on the normalized natural frequencies

n	h (mm)	f									
		m=1	m=2	m=3	m=4	m=5	m=6	m=7	m=8	m=9	m=10
1	4	0.987342	0.998344	0.999150	0.999239	0.999126	0.998877	0.998488	0.997936	0.997187	0.996200
	8	1.017457	1.002314	1.001189	1.001064	1.001222	1.001570	1.002112	1.002882	1.003925	1.005296
	10	1.039470	1.005281	1.002716	1.002431	1.002792	1.003586	1.004822	1.006575	1.008949	1.012063
2	4	0.703630	0.871957	0.951759	0.975393	0.983643	0.986911	0.990347	0.988240	0.987669	0.967049
	8	1.306471	1.155668	1.063869	1.033467	1.022461	1.018042	1.016406	1.016236	1.017012	1.018520
	10	1.617311	1.329290	1.140744	1.074965	1.050634	1.040779	1.037119	1.036736	1.038476	1.041848
3	4	0.668351	0.689651	0.747790	0.817768	0.871135	0.904681	0.924618	0.936328	0.943068	0.946666
	8	1.332152	1.316865	1.271666	1.209859	1.156535	1.119898	1.096866	1.082869	1.074649	1.070211
	10	1.664506	1.636465	1.552608	1.435276	1.331012	1.257365	1.210067	1.180901	1.163611	1.154224
4	4	0.666838	0.669258	0.678386	0.697653	0.725938	0.758091	0.788705	0.814658	0.835105	0.850455
	8	1.333213	1.331515	1.325032	1.310951	1.289271	1.263098	1.236576	1.212792	1.193163	1.177886
	10	1.666447	1.663340	1.651464	1.625576	1.585448	1.536539	1.486412	1.440924	1.402967	1.373143
5	4	0.666696	0.667115	0.668806	0.672865	0.680129	0.690772	0.704192	0.719247	0.734657	0.749341
	8	1.333313	1.333019	1.331832	1.328967	1.323781	1.316043	1.306047	1.294510	1.282338	1.270387
	10	1.666629	1.666092	1.663921	1.658677	1.649169	1.634952	1.616527	1.595176	1.572544	1.550213
6	4	0.666673	0.666772	0.667182	0.668207	0.670166	0.673304	0.677728	0.683375	0.690027	0.697360
	8	1.333329	1.333259	1.332972	1.332253	1.330875	1.328656	1.325503	1.321438	1.316589	1.311169
	10	1.666658	1.666531	1.666007	1.664691	1.662169	1.658106	1.652329	1.644870	1.635958	1.625978
7	4	0.666669	0.666698	0.666820	0.667132	0.667745	0.668768	0.668773	0.672339	0.674931	0.678015
	8	1.333332	1.333312	1.333226	1.333008	1.332577	1.331859	1.330792	1.329340	1.327499	1.325298
	10	1.666664	1.666627	1.666471	1.666071	1.665284	1.663970	1.662017	1.659359	1.655988	1.651952
8	4	0.666667	0.666677	0.666720	0.666830	0.667050	0.667425	0.667997	0.668797	0.669846	0.684687
	8	1.333333	1.333326	1.333296	1.333219	1.333065	1.332802	1.332401	1.331839	1.331101	1.330183
	10	1.666666	1.666653	1.666598	1.666458	1.666175	1.665694	1.664961	1.663933	1.662583	1.660902
9	4	0.666667	0.666671	0.666688	0.666731	0.666820	0.666972	0.667209	0.667547	0.668000	0.668578
	8	1.333333	1.333330	1.333319	1.333288	1.333226	1.333119	1.332954	1.332717	1.332399	1.331993
	10	1.666666	1.666661	1.666640	1.666584	1.666471	1.666275	1.665972	1.665539	1.664957	1.664215
10	4	0.666667	0.666669	0.666676	0.666695	0.666734	0.666801	0.666907	0.667061	0.667271	0.667543
	8	1.333333	1.333332	1.333327	1.333314	1.333286	1.333239	1.333165	1.333057	1.332910	1.332719
	10	1.666666	1.666664	1.666655	1.666631	1.666581	1.666494	1.666358	1.666161	1.665892	1.665544

3.5 Effect of included angle on natural frequencies

The effect of the included angle on the natural frequencies of the OCCS with all four edges simply supported is investigated in this subsection. The included angles are taken as 10°, 20°, 30°, and 40°. The other parameters of the OCCSs are defined in Table 1. The calculation results are presented in Table 6.

Table 6 shows that the included angle exerts a significant influence on the natural frequencies of the OCCS. For most but not all mode numbers, the natural frequencies of the OCCS decrease as the included angle increases.

For mode numbers $n\leq 4$, the natural frequencies of the OCCS vary complicatedly with the included angle. Specifically, for n=1, the natural frequencies of the OCCS increase with increase of the included angle with an exception for m=1. While for mode numbers of (m, n)=(1, 1), (3–5, 2), and (8–10, 3), the highest and the lowest natural frequencies are corresponding to the included angles of 10° and 20°. For

Table 6 Effect of included angle on the normalized natural frequencies

n	θ_0	f									
		m=1	m=2	m=3	m=4	m=5	m=6	m=7	m=8	m=9	m=10
1	10°	1.833643	0.586061	0.373447	0.328835	0.337702	0.368746	0.409710	0.454711	0.500572	0.545492
	20°	0.650374	0.530346	0.574977	0.633181	0.689290	0.738765	0.780580	0.815210	0.843671	0.867061
	40°	1.639736	1.505554	1.364258	1.261729	1.191768	1.144187	1.111222	1.087784	1.070660	1.057822
2	10°	8.478269	5.593907	3.278414	2.164351	1.607030	1.300909	1.120784	1.010546	0.942377	0.901224
	20°	2.133458	1.470109	0.964795	0.760467	0.689125	0.672086	0.678563	0.695676	0.717478	0.740985
	40°	0.756716	1.330352	1.485445	1.464301	1.406585	1.346494	1.292801	1.247216	1.209248	1.177796
3	10°	8.933813	8.526336	7.571226	6.288760	5.095068	4.168734	3.495575	3.012081	2.661652	2.403730
	20°	2.238140	2.154675	1.945955	1.661616	1.400923	1.206963	1.075853	0.991410	0.939108	0.908472
	40°	0.575038	0.693358	0.930898	1.141649	1.258824	1.303366	1.307601	1.292369	1.268813	1.242576
4	10°	8.970993	8.844580	8.585679	8.164468	7.597134	6.945620	6.284364	5.668810	5.126453	4.663528
	20°	2.245315	2.223379	2.174577	2.090618	1.973966	1.838285	1.700768	1.574498	1.466049	1.376907
	40°	0.565008	0.584316	0.639950	0.734560	0.846474	0.949709	1.029706	1.083910	1.116175	1.132090
5	10°	8.982268	8.912902	8.789190	8.603366	8.351733	8.038224	7.675043	7.280104	6.872813	6.470295
	20°	2.247205	2.235991	2.215136	2.182426	2.136475	2.077632	2.008218	1.932000	1.853236	1.775768
	40°	0.563625	0.569627	0.584828	0.613441	0.656148	0.709202	0.766318	0.821361	0.870024	0.910176
6	10°	8.987816	8.941506	8.862870	8.750416	8.603241	8.421803	8.208431	7.967408	7.704612	7.426851
	20°	2.248091	2.240767	2.228114	2.209621	2.184862	2.153684	2.116348	2.073566	2.026445	1.976342
	40°	0.563202	0.566260	0.572669	0.583826	0.600743	0.623551	0.651360	0.682503	0.714988	0.746944
7	10°	8.991074	8.957433	8.901197	8.822255	8.720700	8.597002	8.452159	8.287773	8.106045	7.909685
	20°	2.248604	2.243322	2.234427	2.221813	2.205395	2.185150	2.161161	2.133639	2.102929	2.069498
	40°	0.562998	0.564993	0.568705	0.574595	0.583094	0.594461	0.608688	0.625474	0.644268	0.664369
8	10°	8.993172	8.967503	8.924809	8.865253	8.789120	8.696867	8.589154	8.466878	8.331175	8.183407
	20°	2.248933	2.244914	2.238205	2.228802	2.216709	2.201959	2.184618	2.164799	2.142662	2.118419
	40°	0.562877	0.564334	0.566892	0.570714	0.575968	0.582788	0.591234	0.601268	0.612753	0.625463
9	10°	8.994606	8.974345	8.940693	8.893836	8.834045	8.761694	8.677262	8.581347	8.474661	8.358029
	20°	2.249157	2.245988	2.240716	2.233356	2.223935	2.212494	2.199090	2.183802	2.166729	2.147993
	40°	0.562796	0.563925	0.565853	0.568642	0.572358	0.577060	0.582782	0.589529	0.597263	0.605908
10	10°	8.567290	8.647176	8.776958	8.914042	8.865645	8.807068	8.738665	8.660859	8.574141	8.479065
	20°	2.249317	2.246752	2.242489	2.236545	2.228949	2.219736	2.208954	2.196659	2.182923	2.167826
	40°	0.562739	0.563645	0.565174	0.567347	0.570192	0.573733	0.577985	0.582951	0.588619	0.594959

mode numbers of (m, n)=(2, 2), (4–7, 3), and (7–10, 4), the highest and the lowest natural frequencies are corresponding to the included angles of 10° and 30°. For mode numbers of (m, n)=(6–10, 2), the highest and the lowest natural frequencies are corresponding to the included angles of 40° and 20°.

3.6 Effect of boundary conditions on natural frequencies

Based on the solutions derived in Sections 2.3 and 2.4, the MRRM is employed to calculate the natural frequencies of the OCCS with the two curved edges or the two straight edges simply supported, and the two remaining edges supported by an arbitrary combination of SSE, CE, and FE, such as SSE-SSE, SSE-CE, SSE-FE, CE-CE, CE-FE, and FE-FE. However, for simplicity, cases of the two remaining edges with the same boundary conditions are chosen as calculation examples to investigate the effect of the boundary conditions on the natural frequencies. The basic parameters are defined in Table 1. The boundary conditions of the two remaining edges

SSE-SSE, CE-CE, and FE-FE are respectively denoted as SSEs, CEs, and FEs in the following discussion.

The effects of boundary conditions on natural frequencies of the shell with simply supported curved edges and simply supported straight edges are respectively presented in Tables 7 and 8. In addition, some mode shapes obtained by MRRM are presented in Fig. 6.

It can be observed from Table 7 that, as the two curved edges are simply supported, the natural frequencies corresponding to the three kinds of boundary conditions of the remaining two edges decrease in the order of CEs, SSEs, and FEs for most but not all mode numbers. For mode numbers (m, n)=(1–10, 1) and (5–10, 2), the natural frequencies of the OCCS with the two remaining edges supported by SSEs, CEs, and FEs decrease in sequence.

Table 8 shows that, as the two straight edges are simply supported, the boundary conditions of the remaining two edges have little effect on the natural frequencies of the OCCS. For circumferential mode numbers no more than 5, the natural frequencies with the two remaining edges supported by CEs, SSEs, and FEs decrease in sequence. However, as the circumferential mode number becomes larger than 5, the natural frequencies of the remaining two edges decrease in the order of FEs, CEs, and SSEs.

4 Conclusions

This paper presents analytical solutions and exact natural frequencies for the OCCS with either the two curved edges or the two straight edges simply supported. Based on the DMV thin shell theory, the solutions of the unidirectional traveling wave form for the OCCS with two opposite simply supported edges are obtained. Subsequently, MRRM is applied to derive the equation of natural frequencies of the OCCS, and the golden section search algorithm is employed to obtain the exact natural frequencies. Then, the proposed procedure is verified by the comparison of the present results with those obtained by FEM and MRRM. Finally, the effects of shell length, shell radius, shell thickness, included angle, and the boundary conditions on natural frequencies of the OCCS are investigated. It can be concluded as follows:

Table 7 Effect of boundary conditions (BCs) on normalized natural frequencies of the OCCS with simply supported curved edges

n	BCs	f									
		m=1	m=2	m=3	m=4	m=5	m=6	m=7	m=8	m=9	m=10
1	CEs	0.650209	0.396872	0.335770	0.325678	0.336265	0.357262	0.384180	0.414717	0.447551	0.481844
	FEs	0.132677	0.134774	0.118332	0.122015	0.135258	0.149735	0.165784	0.185119	0.206725	0.230002
2	CEs	2.236561	2.216614	1.555305	1.137218	0.922816	0.813728	0.759557	0.735621	0.729131	0.733066
	FEs	0.365351	0.372434	0.352469	0.310532	0.282759	0.276181	0.280297	0.288188	0.299694	0.314395
3	CEs	1.251485	1.302330	1.369184	1.377907	1.327416	1.250683	1.171769	1.103327	1.050076	1.011764
	FEs	0.317305	0.744775	0.862625	1.018234	1.023109	0.961361	0.930360	0.918448	0.917112	0.913004
4	CEs	1.298686	1.444120	1.701758	1.906069	1.965036	1.912282	1.810122	1.697644	1.592963	1.502596
	FEs	0.396526	0.528519	0.792104	0.824395	0.957390	1.121704	1.113582	1.080289	1.053374	1.042975
5	CEs	1.166778	1.171053	1.181569	1.198809	1.222570	1.251317	1.280532	1.303517	1.315256	1.314679
	FEs	0.492336	0.502621	0.688657	0.832719	0.847081	0.872209	0.994828	1.108522	1.140859	1.124804
6	CEs	1.175744	1.187143	1.210558	1.252169	1.310458	1.367722	1.408114	1.427904	1.429759	1.417899
	FEs	0.563720	0.568074	0.576205	0.744270	0.857595	0.865915	0.874963	0.884681	0.932900	0.997603
7	CEs	1.111433	1.112086	1.113178	1.114673	1.116495	1.118501	1.120460	1.122037	1.122802	1.122272
	FEs	0.527413	0.620668	0.625151	0.632039	0.733061	0.877860	0.883211	0.889104	0.895390	0.901910
8	CEs	1.128719	1.130418	1.133154	1.136688	1.139468	1.127263	1.113835	1.099160	1.083350	1.066620
	FEs	0.473360	0.662329	0.665153	0.669162	0.674380	0.681254	0.768099	0.829467	0.870224	0.894843
9	CEs	1.137716	1.134904	1.132595	1.130707	1.128947	1.127137	1.125185	1.123039	1.120672	1.118070
	FEs	0.522095	0.695960	0.697908	0.700642	0.704159	0.708449	0.713491	0.719262	0.725766	0.733215
10	CEs	1.102108	1.102442	1.102900	1.103340	1.103617	1.103618	1.103283	1.102599	1.101577	1.100244
	FEs	0.562856	0.723601	0.725010	0.726976	0.729490	0.732539	0.736101	0.740149	0.744650	0.749563

Table 8 Effect of boundary conditions (BCs) on normalized natural frequencies of the OCCS with simply supported straight edges

n	BCs	f									
		m=1	m=2	m=3	m=4	m=5	m=6	m=7	m=8	m=9	m=10
1	CEs	1.747624	1.165110	1.043241	1.011418	1.003505	1.001733	1.001527	1.001687	1.001914	1.002145
	FEs	0.209645	0.661458	0.828184	0.912831	0.953015	0.973321	0.983870	0.989704	0.993003	0.994939
2	CEs	1.148320	1.240040	1.157162	1.086803	1.046977	1.026024	1.015300	1.009901	1.007235	1.005968
	FEs	0.947912	0.790859	0.788696	0.842988	0.888826	0.921530	0.944078	0.959539	0.970171	0.977523
3	CEs	1.009118	1.036024	1.064225	1.072524	1.063742	1.049794	1.037216	1.027726	1.021112	1.016692
	FEs	0.993815	0.977108	0.945324	0.920605	0.914808	0.921559	0.932739	0.944111	0.954108	0.962366
4	CEs	1.001433	1.005825	1.012727	1.020354	1.026346	1.029308	1.029379	1.027571	1.024946	1.022232
	FEs	0.996149	0.994489	0.989684	0.982263	0.974072	0.967459	0.963736	0.962857	0.964043	0.966422
5	CEs	1.000404	1.001607	1.003545	1.006035	1.008765	1.011363	1.013513	1.015044	1.015941	1.016304
	FEs	0.996607	0.996793	0.995804	0.994163	0.991906	0.989263	0.986592	0.984251	0.982479	0.981363
6	CEs	1.000158	1.000626	1.001383	1.002389	1.003581	1.004880	1.006197	1.007451	1.008579	1.009543
	FEs	1.003336	1.007122	1.011012	1.014972	1.018913	1.022706	1.026215	1.029320	1.031935	1.034017
7	CEs	1.000077	1.000305	1.000678	1.001180	1.001794	1.002496	1.003257	1.004049	1.004845	1.005619
	FEs	1.002175	1.004878	1.007600	1.010317	1.012999	1.015607	1.018096	1.020420	1.022538	1.024417
8	CEs	1.000044	1.000174	1.000388	1.000679	1.001041	1.001463	1.001936	1.002448	1.002985	1.003537
	FEs	1.001483	1.003513	1.005562	1.007593	1.009590	1.011536	1.013412	1.015200	1.016879	1.018434
9	CEs	1.000028	1.000110	1.000246	1.000433	1.000667	1.000945	1.001260	1.001608	1.001982	1.002377
	FEs	1.001048	1.002619	1.004224	1.005817	1.007384	1.008913	1.010396	1.011822	1.013182	1.014468
10	CEs	1.000019	1.000075	1.000169	1.000297	1.000459	1.000653	1.000875	1.001123	1.001394	1.001683
	FEs	1.000762	1.002003	1.003294	1.004582	1.005851	1.007094	1.008304	1.009475	1.010602	1.011678

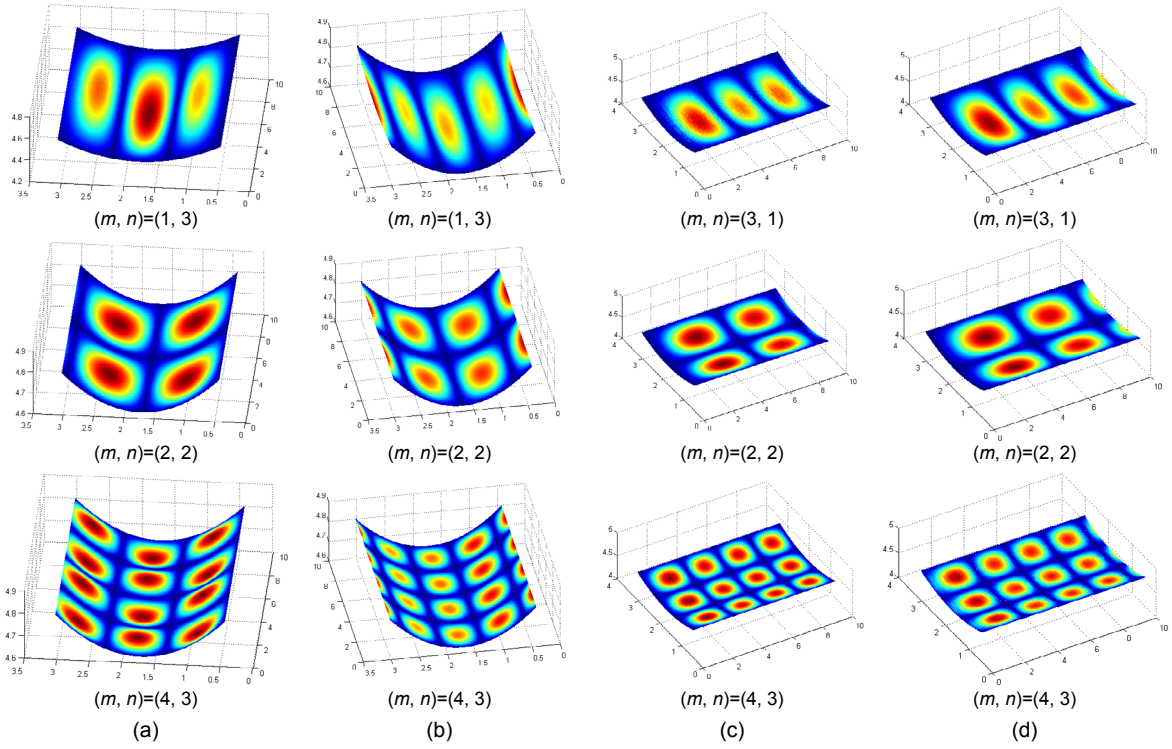

Fig. 6 Mode shapes obtained by MRRM for different boundary conditions
(a) SSE-CE-SSE-CE; (b) SSE-FE-SSE-FE; (c) CE-SSE-CE-SSE; (d) FE-SSE-FE-SSE

1. MRRM is validated and of high precision for vibration analysis of OCCSs.

2. The natural frequencies of the OCCS decrease with the increase of the shell length.

3. The natural frequencies of the OCCS decrease with the increase of the shell radius for most mode numbers.

4. The natural frequencies of the OCCS increase with the increase of the shell thickness. The natural frequencies corresponding to different shell thickness are very close to each other for mode numbers n=1 and 2, while they vary linearly with the shell thickness for mode numbers $n\geq 7$.

5. The natural frequencies of the OCCS decrease rapidly as the included angle increases for most mode numbers.

6. As the two curved edges are simply supported, the natural frequencies corresponding to the three kinds of boundary conditions of the remaining two edges decrease in the order of CEs, SSEs, and FEs for most of the mode numbers.

7. As the two straight edges are simply supported, the boundary conditions of the remaining two edges have little effect on the natural frequencies of the OCCS.

Finally, the exact natural frequencies of the OCCS for various parameters and different boundary conditions are presented in tabular form for easy reference as benchmark values for researchers to verify their numerical methods and for convenient consulting for engineers in practical design.

Acknowledgements

The authors would like to sincerely thank Miss Jing-jing YU from Shengda Trade Economics & Management College of Zhengzhou and Mr. Xian-zhong WANG from Wuhan University of Technology, China for the scientific discussion and suggestions.

References

Cantin, G., Clough, R.W., 1968. A curved, cylindrical-shell, finite element. *AIAA Journal*, **6**(6):1057-1062. http://dx.doi.org/10.2514/3.4673

Chen, M., Mao, H.Y., Sun, G.J., 2005. The effects of damping on the transient response of frames using the method of reverberation ray matrix. *Journal of Shanghai Jiaotong University*, **39**(1):154-156 (in Chinese).

Cheung, Y.K., Li, W.Y., Tham, L.G., 1989. Free vibration analysis of singly curved shell by spline finite strip method. *Journal of Sound and Vibration*, **128**(3):411-422. http://dx.doi.org/10.1016/0022-460X(89)90783-9

Guo, Y.Q., 2008. The Method of Reverberation-ray Matrix and Its Applications. PhD Thesis, Zhejiang University, Hangzhou, China (in Chinese).

Guo, Y.Q., Chen, W.Q., 2008. On free wave propagation in anisotropic layered media. *Acta Mechanica Solida Sinica*, **21**(6):500-506. http://dx.doi.org/10.1007/s10338-008-0860-z

Guo, Y.Q., Fang, D.N., 2014. Analysis and interpretation of longitudinal waves in periodic multiphase rods using the method of reverberation-ray matrix combined with the Floquet-Bloch theorem. *Journal of Vibration Acoustics*, **136**(1):011006. http://dx.doi.org/10.1115/1.4025438

Guo, Y.Q., Chen, W.Q., Pao, Y.H., 2008. Dynamic analysis of space frames: the method of reverberation-ray matrix and the orthogonality of normal modes. *Journal of Sound and Vibration*, **317**(3-5):716-738. http://dx.doi.org/10.1016/j.jsv.2008.03.052

Howard, S.M., Pao, Y.H., 1998. Analysis and experiments on stress waves in planar trusses. *Journal of Engineering Mechanics*, **124**(8):884-891. http://dx.doi.org/10.1061/(ASCE)07339399(1998)124:8(884)

Jiang, J.Q., 2011. Transient responses of Timoshenko beams subject to a moving mass. *Journal of Vibration and Control*, **17**(13):1975-1982. http://dx.doi.org/10.1177/1077546310382808

Jiang, J.Q., Chen, W.Q., Pao, Y.H., 2011. Reverberation-ray analysis of continuous Timoshenko beams subject to moving loads. *Journal of Vibration and Control*, **18**(6):774-784. http://dx.doi.org/10.1177/1077546310397562

Lakis, A.A., Selmane, A., 2000. Hybrid finite element analysis of large amplitude vibration of orthotropic open and closed cylindrical shells subjected to a flowing fluid. *Nuclear Engineering and Design*, **196**(1):1-15. http://dx.doi.org/10.1016/S0029-5493(99)00227-7

Leissa, A.W., 1973. Vibration of shells. Scientific and Technical Information Office, NASA, Washington DC, USA, p.5-175.

Leissa, A.W., Narita, Y., 1984. Vibrations of completely free shallow shells of rectangular planform. *Journal of Sound and Vibration*, **96**(2):207-218. http://dx.doi.org/10.1016/0022-460X(84)90579-0

Li, B.R., Wang, X.Y., Ge, H.L., *et al.*, 2005. Study on applicability of modal analysis of thin finite length cylindrical shells using wave propagation approach. *Journal of Zhejiang University-SCIENCE A*, **6**(10):1122-1127. http://dx.doi.org/10.1631/jzus.2005.A1122

Li, F.M., Liu, C.C., Shen, S., *et al.*, 2012. Application of the method of reverberation ray matrix to the early short time transient responses of stiffened laminated composite plates. *Journal of Applied Mechanics*, **79**(4):04100. http://dx.doi.org/10.1115/1.4006238

Lim, C.W., Liew, K.M., 1995. A higher order theory for vibration of shear deformable cylindrical shallow shells. *International Journal of Mechanical Sciences*, **37**(3):277-295. http://dx.doi.org/10.1016/0020-7403(95)93521-7

Liu, C.C., Li, F.M., Fang, B., *et al.*, 2010. Active control of power flow transmission in finite connected plate. *Journal of Sound and Vibration*, **329**(20):4124-4135. http://dx.doi.org/10.1016/j.jsv.2010.04.027

Liu, C.C., Li, F.M., Liang, T.W., *et al.*, 2011a. Early short time transient response of finite L-shaped Mindlin plate. *Wave Motion*, **48**(5):371-391. http://dx.doi.org/10.1016/j.wavemoti.2011.01.002

Liu, C.C., Li, F.M., Huang, W.H., 2011b. Transient wave propagation and early short time transient responses of laminated composite cylindrical shells. *Composite Structures*, **93**(10):2587-2597. http://dx.doi.org/10.1016/j.compstruct.2011.04.021

Liu, C.C., Li, F.M., Chen, Z.B., *et al.*, 2013. Transient wave propagation in the ring stiffened laminated composite cylindrical shells using the method of reverberation ray matrix. *The Journal of the Acoustical Society of America*, **133**(2):770-780. http://dx.doi.org/10.1121/1.4773261

Liu, G.B., Xie, K.H., 2005. Transient response of a spherical cavity with a partially sealed shell embedded in viscoelastic saturated soil. *Journal of Zhejiang University-SCIENCE A*, **6**(3):194-201. http://dx.doi.org/10.1631/jzus.2005.A0194

Liu, J., Miao, F.X., Sun, G.J., 2006. Modal analysis of frames with reverberation ray matrix method. *Journal of Vibration, Measurement & Diagnosis*, **26**(4):322-323 (in Chinese).

Mecitoglu, Z., Dokmeci, M.C., 1992. Free vibrations of a thin, stiffened, cylindrical shallow shell. *AIAA Journal*, **30**(3):848-850. http://dx.doi.org/10.2514/3.10998

Miao, F.X., Sun, G.J., Chen, K.F., 2013. Transient response analysis of balanced laminated composite beams by the method of reverberation-ray matrix. *International Journal of Mechanical Sciences*, **77**:121-129. http://dx.doi.org/10.1016/j.ijmecsci.2013.09.029

Miao, F.X., Sun, G.J., Chen, K.F., *et al.*, 2015. Reverberation-ray matrix analysis of the transient dynamic responses of asymmetrically laminated composite beams based on the first-order shear deformation theory. *Composite Structures*, **119**:394-411. http://dx.doi.org/10.1016/j.compstruct.2014.09.002

Nayak, A.N., Bandyopadhyay, J.N., 2002. On the free vibration of stiffened shallow shells. *Journal of Sound and Vibration*, **255**(2):357-382. http://dx.doi.org/10.1006/jsvi.2001.4159

Pao, Y.H., Keh, D.C., Howard, S.M., 1999. Dynamic response and wave propagation in plane trusses and frames. *AIAA Journal*, **37**(5):594-603. http://dx.doi.org/10.2514/2.778

Pao, Y.H., Su, X.Y., Tian, J.Y., 2000. Reverberation matrix method for propagation of sound in a multilayered liquid. *Journal of Sound and Vibration*, **230**(4):743-760. http://dx.doi.org/10.1006/jsvi.1999.2675

Press, W.H., Teukolsky, S.A., Vetterling, W.T., *et al.*, 1992. Numerical Recipies in C: the Art of Scientific Computing, 2nd Edition. Cambridge University Press, Cambridge, UK, p.397-401.

Price, N.M., Liu, M., Taylor, R.E., *et al.*, 1998. Vibrations of cylindrical pipes and open shells. *Journal of Sound and Vibration*, **218**(3):361-387. http://dx.doi.org/10.1006/jsvi.1998.1862

Qatu, M.S., 2002. Recent research advances in the dynamic behavior of shells: 1989–2000, Part 1: laminated composite shells. *Applied Mechanics Reviews*, **55**(4):325-350. http://dx.doi.org/10.1115/1.1483079

Qatu, M.S., Sullivan, R.W., Wang, W.C., 2010. Recent research advances on the dynamic analysis of composite shells: 2000–2009. *Composite Structures*, **93**(1):14-31. http://dx.doi.org/10.1016/j.compstruct.2010.05.014

Qiao, H., Chen, W.Q., 2011. Analysis of the penalty version of the Arlequin framework for the prediction of structural responses with large deformations. *Journal of Zhejiang University-SCIENCE A (Applied Physics & Engineering)*, **12**(7):552-560. http://dx.doi.org/10.1631/jzus.A1000519

Selmane, A., Lakis, A.A., 1997a. Dynamic analysis of anisotropic open cylindrical shells. *Computers & Structures*, **62**(1):1-12. http://dx.doi.org/10.1016/S0045-7949(96)00280-5

Selmane, A., Lakis, A.A., 1997b. Vibration analysis of anisotropic open cylindrical shells subjected to a flowing fluid. *Journal of Fluids and Structures*, **11**(1):111-134. http://dx.doi.org/10.1006/jfls.1996.0069

Sewall, J.L., 1967. Vibration analysis of cylindrically curved panels with simply supported or clamped edges and comparison with some experiments. Technical Report No. NASA TN D-3791, Langley Research Center, NASA, Washington DC, USA.

Singh, A.V., Shen, L.B., 2005. Free vibration of open circular cylindrical composite shells with point supports. *Journal of Aerospace Engineering*, **18**(2):120-128. http://dx.doi.org/10.1061/(ASCE)08931321(2005)18:2(120)

Su, X.Y., Tian, J.Y., Pao, Y.H., 2002. Application of the reverberation-ray matrix to the propagation of elastic waves in a layered solid. *International Journal of Solids and Structures*, **39**(21-22):5447-5463. http://dx.doi.org/10.1016/S0020-7683(02)00358-X

Su, Z., Jin, G.Y., Ye, T.G., 2014. Free vibration analysis of moderately thick functionally graded open shells with general boundary conditions. *Composite Structures*, **117**:169-186. http://dx.doi.org/10.1016/j.compstruct.2014.06.026

Suzuki, K., Leissa, A.W., 1986. Exact solutions for the free vibrations of open cylindrical shells with circumferentially varying curvature and thickness. *Journal of Sound and Vibration*, **107**(1):1-15. http://dx.doi.org/10.1016/0022-460X(86)90278-6

Tian, J.Y., Su, X.Y., 2000. Transient axisymmetric elastic waves in finite orthotropic cylindrical shells. *Acta Scientiarum Naturalium Universitatis Pekinensis*, **36**(3):365-372 (in Chinese).

Tian, J.Y., Xie, Z.M., 2009. A hybrid method for transient wave propagation in a multilayered solid. *Journal of Sound and Vibration*, **325**(1-2):161-173. http://dx.doi.org/10.1016/j.jsv.2009.02.041

Tian, J.Y., Li, Z., Su, X.Y., 2003. Crack detection in beams by wavelet analysis of transient flexural waves. *Journal of Sound and Vibration*, **261**(4):715-727. http://dx.doi.org/10.1016/S0022-460X(02)01001-5

Toorani, M.H., Lakis, A.A., 2001. Shear deformation in dynamic analysis of anisotropic laminated open cylindrical shells filled with or subjected to a flowing fluid. *Computer Methods in Applied Mechanics and Engineering*, **190**(37-38):4929-4966. http://dx.doi.org/10.1016/S0045-7825(00)00357-1

Vajda, S., 2007. Fibonacci and Lucas Numbers, and the Golden Section: Theory and Applications. Dover Publications, New York, USA.

Ye, T.G., Jin, G.Y., Su, Z., *et al.*, 2014a. A unified Chebyshev–Ritz formulation for vibration analysis of composite laminated deep open shells with arbitrary boundary conditions. *Archive of Applied Mechanics*, **84**(4):441-471. http://dx.doi.org/10.1007/s00419-013-0810-1

Ye, T.G., Jin, G.Y., Chen, Y.H., *et al.*, 2014b. A unified formulation for vibration analysis of open shells with arbitrary boundary conditions. *International Journal of Mechanical Sciences*, **81**:42-59. http://dx.doi.org/10.1016/j.ijmecsci.2014.02.002

Yu, C.L., Chen, Z.P., Wang, J., *et al.*, 2012. Effect of weld reinforcement on axial plastic buckling of welded steel cylindrical shells. *Journal of Zhejiang University-SCIENCE A (Applied Physics & Engineering)*, **13**(2):79-90. http://dx.doi.org/10.1631/jzus.A1100196

Yu, S.D., Cleghorn, W.L., Fenton, R.G., 1995. On the accurate analysis of free vibration of open circular cylindrical shells. *Journal of Sound and Vibration*, **188**(3):315-336. http://dx.doi.org/10.1006/jsvi.1995.0596

Yu, Y., 2007a. Stress wave propagation and study on influencing factor in frame structure embedded partially in soil. *Chinese Journal of Computational Mechanics*, **24**(5):659-663 (in Chinese).

Yu, Y., 2007b. Studies on wave responses of a defective frame structure embedded partially in soil and influence factors. *Journal of Vibration Engineering*, **20**(2):194-199 (in Chinese).

Zhang, L., Xiang, Y., 2006. Vibration of open circular cylindrical shells with intermediate ring supports. *International Journal of Solids and Structures*, **43**(13):3705-3722. http://dx.doi.org/10.1016/j.ijsolstr.2005.05.058

Zhang, X.M., Liu, G.R., Lam, K.Y., 2001. Frequency analysis of cylindrical panels using a wave propagation approach. *Applied Acoustics*, **62**(5):527-543. http://dx.doi.org/10.1016/S0003-682X(00)00059-1

Zhou, Y.Y., Chen, W.Q., Lv, C.F., *et al.*, 2009. Reverberation-ray matrix analysis of free vibration of piezoelectric laminates. *Journal of Sound and Vibration*, **326**(3-5):821-836. http://dx.doi.org/10.1016/j.jsv.2009.05.008

Zhu, J., Ye, G.R., Xiang, Y.Q., *et al.*, 2011. Recursive formulae for wave propagation analysis of FGM elastic plates via reverberation-ray matrix method. *Composite Structures*, **93**(2):259-270. http://dx.doi.org/10.1016/j.compstruct.2010.07.007

Zhu, J., Chen, W.Q., Ye, G.R., 2012. Reverberation-ray matrix analysis for wave propagation in multiferroic plates with imperfect interfacial bonding. *Ultrasonics*, **52**(1):125-132. http://dx.doi.org/10.1016/j.ultras.2011.07.004

中文概要

题　目： 开口圆柱壳的回传射线矩阵法精确自由振动分析

目　的： 开口圆柱壳作为板壳组合结构的组成部分被广泛应用于工程实践中。本文探讨开口圆柱壳结构参数（长度、半径、厚度和夹角等）和边界条件对其振动特性的影响，这对工程结构的减振设计具有重要意义。通过推导开口圆柱壳的解析解及其求解过程，建立加筋开口圆柱壳和板−壳耦合模型振动分析的理论基础。

创新点： 1. 推导行波与驻波结合形式的解析解；2. 建立回传射线矩阵法分析开口圆柱壳结构振动的流程；3. 分析得到大模态数下开口圆柱壳固有频率随壳厚线性变化；直边简支时，曲边边界条件对固有频率影响不大。

方　法： 1. 基于 Donnell-Mushtari-Vlasov （DMV）薄壳理论，推导两对边简支的开口圆柱壳行波与驻波结合形式的解析解；2. 基于回传射线矩阵法原理，推导出开口圆柱壳的固有频率方程；3. 采用黄金分割法求解开口圆柱壳的固有频率方程，得到精确的固有频率；4. 分析开口圆柱壳不同结构参数和边界条件对固有频率的影响。

结　论： 1. 回传射线矩阵法适用于开口圆柱壳的振动分析且具有很高的精度；2. 开口圆柱壳的固有频率随其长度的增加而减小；3. 对于绝大部分模态数，开口圆柱壳的固有频率随其半径的增加而减小；4. 开口圆柱壳的固有频率随壳厚的增加而增加，当周向模态数 n=1 和 2 时，不同壳厚的开口圆柱壳固有频率相差很小，当周向模态数 n≥7 时，开口圆柱壳的固有频率随壳厚线性变化；5. 对于绝大多数模态数，开口圆柱壳的固有频率随夹角的增大而快速减小；6. 对于两曲边简支的开口圆柱壳，其固有频率从高到低对应两直边的边界条件为固支、简支和自由；7. 对于两直边简支的开口圆柱壳，两曲边的边界条件对其固有频率的影响不大。

关键词： 开口圆柱壳；回传射线矩阵法；自由振动分析；DMV 薄壳理论；解析波动形式解